


RESEARCH

Open Access



Genetic inactivation of SARM1 axon degeneration pathway improves outcome trajectory after experimental traumatic brain injury based on pathological, radiological, and functional measures

Donald V. Bradshaw Jr.^{1,2}, Andrew K. Knutsen^{3,4}, Alexandru Korotcov^{3,4}, Genevieve M. Sullivan², Kryslaine L. Radomski^{2,4}, Bernard J. Dardzinski^{3,4,6}, Xiaomei Zi², Dennis P. McDaniel⁵ and Regina C. Armstrong^{1,2,4*} 

Abstract

Traumatic brain injury (TBI) causes chronic symptoms and increased risk of neurodegeneration. Axons in white matter tracts, such as the corpus callosum (CC), are critical components of neural circuits and particularly vulnerable to TBI. Treatments are needed to protect axons from traumatic injury and mitigate post-traumatic neurodegeneration. SARM1 protein is a central driver of axon degeneration through a conserved molecular pathway. *Sarm1*^{-/-} mice with knockout (KO) of the *Sarm1* gene enable genetic proof-of-concept testing of the SARM1 pathway as a therapeutic target. We evaluated *Sarm1* deletion effects after TBI using a concussive model that causes traumatic axonal injury and progresses to CC atrophy at 10 weeks, indicating post-traumatic neurodegeneration. *Sarm1* wild-type (WT) mice developed significant CC atrophy that was reduced in *Sarm1* KO mice. Ultrastructural classification of pathology of individual axons, using electron microscopy, demonstrated that *Sarm1* KO preserved more intact axons and reduced damaged or demyelinated axons. Longitudinal MRI studies in live mice identified significantly reduced CC volume after TBI in *Sarm1* WT mice that was attenuated in *Sarm1* KO mice. MR diffusion tensor imaging detected reduced fractional anisotropy in both genotypes while axial diffusivity remained higher in *Sarm1* KO mice. Immunohistochemistry revealed significant attenuation of CC atrophy, myelin loss, and neuroinflammation in *Sarm1* KO mice after TBI. Functionally, *Sarm1* KO mice exhibited beneficial effects in motor learning and sleep behavior. Based on these findings, *Sarm1* inactivation can protect axons and white matter tracts to improve translational outcomes associated with CC atrophy and post-traumatic neurodegeneration.

Keywords: Chronic traumatic brain injury, SARM1, Sterile alpha and Toll, interleukin-1 receptor containing motif 1, White matter, Corpus callosum atrophy, Magnetic resonance imaging

Background

Traumatic brain injury (TBI) results in long term disability in more severe cases and can cause persistent symptoms even in patients who receive a “mild” diagnosis [42, 67, 72]. TBI may also lead to post-traumatic neurodegeneration and increase the risk for co-morbid

*Correspondence: regina.armstrong@usuhs.edu

² Department of Anatomy, Physiology and Genetics, F. Edward Hebert School of Medicine, Uniformed Services University of the Health Sciences, 4301 Jones Bridge Rd., Bethesda, MD 20814, USA
Full list of author information is available at the end of the article



© The Author(s) 2021. **Open Access** This article is licensed under a Creative Commons Attribution 4.0 International License, which permits use, sharing, adaptation, distribution and reproduction in any medium or format, as long as you give appropriate credit to the original author(s) and the source, provide a link to the Creative Commons licence, and indicate if changes were made. The images or other third party material in this article are included in the article's Creative Commons licence, unless indicated otherwise in a credit line to the material. If material is not included in the article's Creative Commons licence and your intended use is not permitted by statutory regulation or exceeds the permitted use, you will need to obtain permission directly from the copyright holder. To view a copy of this licence, visit <http://creativecommons.org/licenses/by/4.0/>. The Creative Commons Public Domain Dedication waiver (<http://creativecommons.org/publicdomain/zero/1.0/>) applies to the data made available in this article, unless otherwise stated in a credit line to the data.

neurodegenerative diseases, such as Alzheimer's disease [16, 19, 31, 73]. In patients with moderate-severe TBI, diffuse axonal injury has been shown to predict the extent of post-traumatic neurodegeneration, based on MRI volumetric and diffusion tensor imaging (DTI) data [30]. The strongest relationship was found in central white matter tracts, including the corpus callosum (CC). The CC is one of the main structures exhibiting atrophy across patients with complicated mild to severe TBI [16, 31]. Furthermore, DTI tractography demonstrated disrupted fiber tract continuity in anterior CC regions after concussions while broad areas of disrupted tracts were found throughout the CC in patients with MRI findings of diffuse axonal injury [38]. Ex vivo MRI of a patient who died 26 days after TBI demonstrated that white matter tract disruptions detected by DTI correlated with neuropathological identification of axonal injury [69].

Long axons in white matter tracts are particularly vulnerable to damage in all forms of closed head TBI [11, 40, 57, 78]. At an early stage of damage, axons can exhibit focal swellings yet longitudinal in vitro and in vivo imaging has shown the potential to recover [32, 37, 68]. Once mechanical or molecular processes fragment the axon, then the distal axon irreversibly degrades by Wallerian degeneration [32, 37, 54, 56, 68]. The majority of axon damage is due to secondary mechanisms of damage that can cause axons to initiate Wallerian degeneration for weeks or more after the initial TBI event [13, 54, 56]. Irreversible axonal injury leads to disconnection between brain regions and disruption of neural circuits that may contribute to diverse TBI symptoms [33, 59]. To improve outcomes for patients after TBI, research is needed to identify approaches to protect against axon degeneration and, further, to determine whether acute axon protection can reduce post-traumatic neurodegeneration.

Wallerian degeneration is an "active program of axon self-destruction" [76]. After injury or mitochondrial dysfunction, the SARM1 (sterile alpha and Toll/interleukin-1 receptor motif-containing 1) protein executes a highly conserved molecular axon degeneration pathway [27, 48, 70, 84]. Injury releases SARM1 from an auto-inhibited state that is found in healthy axons [22, 76, 80]. Active SARM1 is a glycohydrolase which depletes nicotinamide adenine dinucleotide (NAD⁺) that is critical for energy stores in axons [18, 23, 26]. Loss of sufficient NAD⁺ leads to a cascade of axon destruction in which ionic imbalance leads to cytoskeletal and structural breakdown within the axon [25, 26, 85].

Deletion of the *Sarm1* gene provides a genetic proof-of-concept to examine the effects of long-term inactivation of this axon degeneration pathway in chronic TBI and to evaluate the relationship of axonal injury to post-traumatic neurodegeneration. Knockout of *Sarm1*

in cultured human sensory neurons and in live mice reduced axon damage in models of peripheral neuropathy induced by trauma or chemotherapy [14, 24, 26, 70]. In multiple models of TBI, *Sarm1* knockout (KO) mice exhibited significantly reduced axon damage at acute and late phase time points [35, 52, 58, 96]. Long-term studies of TBI in mice can model post-traumatic neurodegeneration that includes atrophy of the CC [47, 53, 64]. Initial results from our prior studies provided the first evidence that *Sarm1* deletion may reduce both late stage axon damage and CC atrophy [52].

We now focus on CC atrophy as an important translational outcome measure of post-traumatic neurodegeneration. We evaluate the effect of *Sarm1* deletion on axon damage, demyelination, and neuroinflammation on the progression of CC atrophy after closed head TBI. We use longitudinal MRI to detect changes in CC volume and white matter integrity in live mice, which provides a highly translational outcome measure of prolonged *Sarm1* inactivation. To demonstrate whether the pathological effects of *Sarm1* deletion have a meaningful impact on complex functions, we assess motor skill learning and sleep behavior. This experimental design provides a rigorous and translationally relevant screen to evaluate the impact of *Sarm1* deletion on long-term outcome measures after TBI.

Materials and methods

Mice

All mice were treated in accordance with guidelines of the Uniformed Services University of the Health Sciences and the National Institutes of Health Guide for the Care and Use of Laboratory Animals. Mice were socially housed with 2–5 mice per 35 cm × 16.5 cm × 18 cm cages containing enrichment objects. Mice were maintained on a standard 12 h cycle of daytime light (6:00–18:00). *Sarm1*^{-/-} knockout (KO) mice, B6.129 × 1-Sarm1tm1Aidi/J (RRID:IMSR_JAX:018069) were originally obtained from The Jackson Laboratory. *Sarm1* KO mice were generated by targeted mutation that replaced exons 3 through 6 with a neo cassette in the reverse orientation and absence of SARM1 protein in the brain was confirmed by western blot [43]. *Sarm1* KO mice were backcrossed to C57BL/6 mice for 15 generations before arrival at The Jackson Laboratory and then crossed at least once to C57BL/6 J mice. For our studies, *Sarm1* KO mice were crossed to C57BL/6 J mice and then heterozygotes were bred to generate littermates used in experiments. *Sarm1* is highly expressed in the brain; lack of detectable SARM1 protein in *Sarm1* KO mice does not produce gross or microscopic brain pathology [28, 43]. The colony was maintained at Charles River Laboratories (Wilmington, MA) where ear biopsies were genotyped

using a 3-primer allele specific PCR assay that targets the mutated *Sarm1* region. Experimental mice were acclimated for 3 days after shipment and prior to the start of experiments.

The total number of mice used in experiments was *Sarm1* WT (n=66; 33 male, 33 female) and *Sarm1* KO (n=75; 34 male, 41 female) littermates. The specific number of mice used for quantification in each experiment is shown by symbols on the graphs and/or stated in each figure legend. Mice used for EM or for Miss-step wheel running were not included in any other analyses. Mice used for MRI were perfused and included in post-imaging tissue analysis. Immunohistochemical analyses included MRI mice and sleep study mice as well as additional cohorts to fulfill the conditions and sample sizes needed for the sleep analysis.

TBI and sham procedures

The TBI model has been characterized in our previous studies [52, 61]. This concussive, closed head injury model results in pathology under the impact site at bregma in the CC and the adjacent cingulum [53, 83]. Under 2% isoflurane anesthesia, 8–10 week old mice received a single impact onto the skull at bregma (i.e. 0 ML, 0 AP, 0 DV) using an ImpactOne stereotaxic impactor (Leica Biosystems, Buffalo Grove, IL) with a 3-mm-diameter tip (velocity set at 4.0 m/s; depth of 1.5 mm; dwell time of 100 ms). Sham mice received the same procedure without the impact. Righting reflex demonstrated a significant injury effect of longer time to righting after TBI, as compared to sham procedures, which did not differ with *Sarm1* genotype or sex (Additional File 1: Figure S1). The predetermined study design criteria required exclusion of three mice for depressed skull fracture and/or impactor malfunction.

Electron microscopy

Transmission electron microscopy (EM) was used to analyze axon and myelin subcellular structure, which can reveal a broad range of axon and myelin pathology [53, 61]. Cohorts consisted of *Sarm1* WT sham (n=9; 4 female, 5 male) and TBI (n=8; 4 female, 4 male) along with *Sarm1* KO sham (n=7; 3 female, 4 male) and TBI (n=9; 5 female, 4 male). Mice were sacrificed at 10 weeks after sham or TBI procedure. Mice were anesthetized with ketamine/xylazine before transventricular cardiac perfusion with 4% paraformaldehyde (Electron Microscopy Sciences, Hatfield, PA; Cat #19210) and 2.5% glutaraldehyde (Electron Microscopy Sciences; Cat #16210) in 0.1 M phosphate buffer. After overnight post-fixation, brains were cut into sagittal (40 μ m) sections using a Leica VT-1200 vibrating blade microtome (Leica Biosystems, Buffalo Grove, IL). Parasagittal sections were

immersed in 2% osmium tetroxide (OsO₄; Electron Microscopy Sciences; Cat #19100) infiltrated with Spurr epoxy resin (Electron Microscopy Sciences; Cat #14300), flat-embedded and then polymerized at 70 °C for 11 h. Thin sections (~70 nm) were cut on an Ultracut UC6 ultramicrotome (Leica Biosystems). Copper grids containing thin sections were post-stained for 20 min in 2% aqueous uranyl acetate (Electron Microscopy Sciences; Cat #22400) and for 5 min in Reynolds lead citrate (Reynolds, 1963).

Quantification of sagittal CC width and electron microscopy analysis

Prior to thin sectioning, resin-embedded 40 μ m sagittal sections approximately 200 μ m lateral to the midline were osmicated to stain myelin and imaged in bright field on an Olympus IX-70 microscope. CC width was measured across the superior to inferior borders in five locations at ~100 μ m intervals across a 0.5 mm rostro-caudal region centered under bregma. This region-of-interest (ROI) consistently exhibits traumatic axonal injury in this TBI model, as evidenced by dispersed damaged axons among adjacent intact axons, and matches the EM analysis performed in our previous work with this *Sarm1* line of mice [52, 53].

Thin sections for EM analysis were then cut from within the CC ROI of the 40 μ m thick sections. The EM grids of sagittal thin sections were reviewed on a JEOL JEM-1011 transmission electron microscope (JEOL USA Inc., Peabody, MA) and images were acquired using an AMT XR50S-A digital camera (Advanced Microscopy Techniques, Woburn, MA). Images were taken at 5000 \times magnification and 8–10 images per animal were quantified for classification of axon and myelin pathology. For each image, a 17 μ m \times 12.5 μ m region defined the counting frame, within which >120 axons were quantified. All axons within the counting frame were counted. Axons partially crossing the top and right lines were included while those partially crossing the left and bottom line were excluded. Axons were classified as intact axons, de/unmyelinated axons, axons with abnormal mitochondria, or damaged axons [52, 53, 61]. Damaged axons were defined as axons with cytoskeletal disruption or axons with accumulated vesicles and debris. Mitochondria that appeared swollen encompassed >50% of the area of the axon cross-section and were considered abnormal. De/unmyelinated axons were >0.3 μ m in diameter and lacked detectable compact myelin, but otherwise appeared intact. Axons without myelin and with a diameter <0.3 μ m were excluded as this axon size is typically unmyelinated in the CC of healthy adult mice [81]. TBI-induced demyelination was inferred when de/unmyelinated axon counts were significantly greater

after TBI, as compared to sham. Myelin outfoldings were identified as myelin extending out from an axon and folding back onto itself to form double layered or redundant myelin [61] but were not significantly induced by TBI at this 10 week time point in mice of either genotype (data not shown). Additional images were taken at 10,000–15,000 \times for illustration of pathological features.

Magnetic resonance imaging (MRI) analysis of CC volume and microstructure

MRI with multi-spin-echo for T2 relaxation time mapping, high resolution 3D proton density (PD-w) for volumetric calculations and diffusion tensor images (DTI) were acquired to assess the longitudinal effects of *Sarm1* knockout in the CC ROI following TBI. Longitudinal MRI studies were conducted in live mice with repeated scans of the same mouse at baseline (prior to TBI) and at 3 days and 10 weeks post-TBI. Mice were scanned on a 7 T Bruker BioSpec 70/20 USR Magnetic Resonance Imaging System with a 660 mT/m, 12 cm diameter gradient coil, 86 mm quadrature TX/RX coil, and Bruker Mouse head 4 channel receive coil array (Bruker BioSpin GmbH, Reinsetten, Germany). Mice were anesthetized in an induction chamber with a mixture of 4% isoflurane in medical air and maintained with 1.5–1.75% isoflurane in medical air delivered by nose cone during the MRI procedures. Respiration rate (range 40–70 BPM, maintained by adjusting isoflurane concentration) and temperature were continuously monitored throughout the experiments. MRI slices were positioned using a sagittal localizer so that coronal slices were oriented perpendicular to the length of the CC axis and each brain was aligned with the midline crossing of the anterior commissure within in the same coronal slice [82, 87, 95].

A whole brain T2 relaxation time map was generated from a two-dimensional rapid acquisition with relaxation enhancement (2D RARE, coronal [34] using the following parameters: TR=4000 ms, echo time (TE)=10, 30, 50, 70, 90, 110 ms, echo train length (ETL)=2, number of averages NA=4, field of view (FOV) 14 mm \times 14 mm, matrix 112 \times 112, in-plane resolution 125 μ m \times 125 μ m, slice thickness 750 μ m, number of slices NS=21, no fat suppression, BW 36 kHz, time 14:56 min. Additionally, a high resolution proton density weighted (PD-w) 3D MRI was acquired to measure CC volumetrics using the following parameters: 3D RARE, TR=2500 ms, TE=30 ms, ETL=8, number of averages NA=1, FOV 18 mm \times 14 mm \times 11 mm, matrix 144 \times 112 \times 88, 125 μ m isotropic resolution, no fat suppression, BW 36 kHz, time 55:25 min. DTI data was acquired using the following parameters: 2D 2-shot echo planar imaging (EPI), TR=3000 ms, TE=27, NA=2, 4 B0 and 30 non-collinear diffusion directions, b=600, 1200 s/mm², δ =5

ms, Δ =12 ms, FOV 14 mm \times 14 mm, in-plane resolution 175 μ m \times 175 μ m, matrix 80 \times 80, slice thickness 750 μ m, number of slices NS=21, fat suppression, BW 300 kHz, time 12:48 min.

The multi-echo T2-w images were converted to the NIFTI file format using a custom script in Matlab. A bias field correction was performed on the 30 ms echo time image using the `N4BiasFieldCorrection` command in the Advanced Normalization Toolkit (ANTs) [7]. The computed bias field was then applied to the other echo times (10, 50, 70, 90, 110 ms). Estimates of T2-decay (T2) and amplitude (S_0) images (maps) were obtained using a nonlinear fit to the equation $S_i(TE) = S_0 \cdot \exp(-TE_i/T2)$, where S_i is the signal intensity for echo time TE_i . The T2-map and amplitude values were fed into a deep learning algorithm to create a brain mask [74, 82, 95]. Brain masks were manually corrected as needed. The ROI in the CC was drawn manually using VivoQuant software (inviCRO, Boston, MA). The CC ROI was defined as extending from the midline bilaterally to the point of ventral curvature in the external capsule (Additional File 1: Figure S2), as in our previous studies [82, 95].

DTI were processed using the TORTOISE v3.2.0 software package [65, 71]. Motion correction, eddy current correction, and EPI distortion correction were performed using the `DIFFPREP` function. Tensors were computed using a nonlinear tensor fit with `RESTORE`, and fractional anisotropy (FA), trace (TR), axial diffusivity (AD), and radial diffusivity (RD) were computed from the diffusion tensor images. An ROI was drawn manually in the CC within the slice under the impact site at bregma (Additional File 1: Figure S2), and average CC values of FA, TR, AD, and RD were computed. TR did not show an effect of injury or genotype (data not shown).

To calculate volume change in the CC the 125 μ m isotropic 3D PD-weighted image slices were converted to NIFTI file format using a custom script in Matlab. A bias field correction was performed using the `N4BiasFieldCorrection` command in the Advanced Normalization Toolkit (ANTs) [7]. The brain mask from the multi-spin-echo T2 image set was transformed to the 3D PD-w imaging using rigid registration and linear interpolation and thresholded at 0.5 to create a new binary mask. A template was created from the baseline scans using the `antsMultivariateTemplateConstruction2.sh` script [8]. Each image for each time point was then registered to the template using the nonlinear registration algorithm in ANTs [7]. Registration parameters were selected based on the approach described by Anderson et al. [3]. Voxel-wise maps of volume change were created using the `CreateJacobianDeterminantImage` function in the ANTs toolkit. A ROI was drawn manually in the CC on each of seven 125 μ m coronal image slices (Additional

File 1: Figure S2) that encompassed the CC over the lateral ventricle and under the site of injury within the +0.5 and -0.5 mm window relative to bregma. The average value of volume change was then computed.

Immunohistochemistry

Immunohistochemical analysis used cohorts of *Sarm1* littermates perfused at 10 weeks after the TBI or sham procedure for *Sarm1* WT sham (n=7; 3 female, 4 male) and TBI (n=11; 6 female, 5 male) along with *Sarm1* KO sham (n=6; 2 female, 4 male) and TBI (n=11; 5 female, 6 male). *Sarm1* mice were perfused with 4% paraformaldehyde and brains cut as 14 μ m-thick coronal cryosections for immunohistochemistry, as in prior studies [82]. Myelin was detected by immunolabelling for myelin oligodendrocyte glycoprotein (MOG; polyclonal mouse anti-MOG; 1:100; Millipore, Burlington MA; Cat# MAB5680, RRID: AB_1587278) followed by incubation with Cy3-conjugated secondary antibody (1:50 Jackson ImmunoResearch, West Grove, PA; Cat# 715-166-150, RRID: AB_2340816). Astrocytes and microglia were immunolabeled as a double stain in separate fluorescent channels. Astrocytes were evaluated by immunostaining for glial fibrillary acidic protein (GFAP; monoclonal mouse anti-GFAP; 1:500 [82]; Millipore, Burlington, MA; Cat# MAB3402, RRID:AB_94844) with secondary incubation using AlexaFluor-594-conjugated secondary antibody (1:400, Jackson ImmunoResearch; Cat# 711-587-003, RRID: AB_2340623). Microglia/macrophages were identified using polyclonal rabbit antibody against ionized calcium binding adaptor molecule 1 (IBA1; 1:500; Wako, Richmond, VA; Cat# 019-19741, RRID:AB_839504) followed by incubation with AlexaFluor-488-conjugated secondary antibody (1:400, Jackson ImmunoResearch Cat# 715-546-151, RRID: AB_2340850). Axon damage was detected using a rabbit polyclonal antibody against β -amyloid precursor protein (β -APP CT695; 1:00, ThermoFisher Cat# 51-2700, RRID: AB_87659) followed by incubation with Cy3 conjugated donkey anti-rabbit IgG (1:100, Jackson ImmunoResearch Cat# 711-166-152, RRID: AB_2313568). All tissue sections were counterstained with DAPI nuclear stain (Sigma-Aldrich, St. Louis, MO; Cat# D9542). Primary antibodies immunolabeled the target structures and cell types without inappropriate co-localization or non-specific signal. Secondary antibodies resulted only low non-specific signal in the absence of an appropriate primary antibody.

Immunohistochemical analysis of coronal CC width, myelination, and neuroinflammation

Images within the CC ROI were acquired with a 10 \times objective on an Olympus IX-70 microscope using a

SPOT RT3 camera. For quantification in coronal images, the CC ROI extended from the midline laterally to under the peak of the cingulum at coronal levels between +0.5 and -0.5 mm relative to bregma. The CC width (superior-inferior thickness) was measured as the average of measurements taken at the midline and bilaterally at ~200 μ m lateral to the midline, under the peak of the cingulum, and ~200 μ m lateral to the peak of the cingulum using MOG staining (Additional File 1: Figure S2). ImageJ software was used to threshold fluorescence levels to quantify the area of immunolabeling above background within the CC ROI area to determine the percent area [5, 52]. Images were also acquired with a 40 \times objective to classify the morphology of IBA1 immunolabeled cells as resting or activated cells [61, 83, 95]. Quantification included 4–6 sections per mouse.

Motor skill learning task

The Miss-step wheel motor assay was performed using a protocol previously described [82]. The Miss-step wheel motor assay has been shown to engage the CC and be sensitive to changes in myelination [36, 60, 62]. From 8 to 10 weeks post TBI, mice were singly housed in home cages with a Miss-step running wheel equipped with an optical sensor to detect wheel revolutions (Mouse Miss-step Activity Wheel system, Cat# 80821, Lafayette Instruments, Lafayette, IN). The Miss-step running wheels have 16 rungs missing from a standard wheel so that the remaining 22 rungs are distributed in an irregular interval pattern [36]. Mouse whiskers were clipped so that avoiding miss-steps was dependent on learning to follow the rung located on the prior step by bringing the hind paw forward to grasp the rung used by the forepaw [60]. Activity Wheel Counters (Cat# 86061) with Activity Wheel Monitor software (Lafayette Instruments) counted wheel revolutions at 6 min intervals during the “lights on” sleeping phase and 1 min intervals during the “lights off” awake active phase. An infrared sensor records each rung that passes and the software uses the rung number and wheel dimensions to calculate the velocity, distance, and continuity of running intervals. Results were exported to a Microsoft Excel file every 24 h. The first week of exposure to the Miss-step wheels has been shown to have a steep learning curve, consistent with mastering this motor skill [36, 60]. After this learning phase, the velocity is typically plateaus to a more stable level across the second week [62, 82]. The mice are removed for cage cleaning between days 7 and 8.

Sleep/wake pattern

Sleep pattern data was collected using a non-invasive automated scoring system (Signal Solutions LLC, Lexington, KY). Mice were single housed during the

8th week following TBI or sham procedures for 72 h and maintained on a standard 12 h cycle of daytime light (6:00–18:00) with continuous data collection. A cage floor matt with piezoelectric sensors recorded 4 s epochs and used the 2–4 Hz breathing rhythm of mice to classify intervals of 30 s or more as asleep or awake [51]. This piezoelectric sensor system compares well with sleep data collected by visual observation and with electrophysiological discrimination of sleep/wake intervals, yet avoids the surgical procedures of electrophysiological techniques that could confound other assessments of TBI [63, 94].

Statistical analysis

Sample sizes were estimated for >80% power based on prior data in *Sarm1* and in C57BL/6 mice [52, 95] (Additional File 1: Figures S2, S3). Mice were randomized to TBI/sham using the RAND function in Microsoft Excel. Investigators not involved in the study coded slide or file numbers to blind those involved in data collection and analysis to genotype and injury condition. GraphPad Prism 8.0 software (RRID: SCR_002798) was used for statistical analysis and graphing. Bar graphs show means with standard error of the mean and symbols for individual mouse values. Student's *t*-test was used for comparison of two conditions (sham vs injury; WT vs KO) at a single time point. Two-way ANOVA was used to determine statistically significant differences when comparing by genotype and injury between groups. Repeated measures two-way ANOVA (RM ANOVA) was used to assess differences between genotypes over time in the longitudinal MRI analysis and within behavioral assessments. Corrections for multiple comparisons used the Holm-Sidak's test. Total distance accumulated during each week of wheel running was compared based on a linear regression model. An alpha-level of *p* value < 0.05 was considered statistically significant.

Results

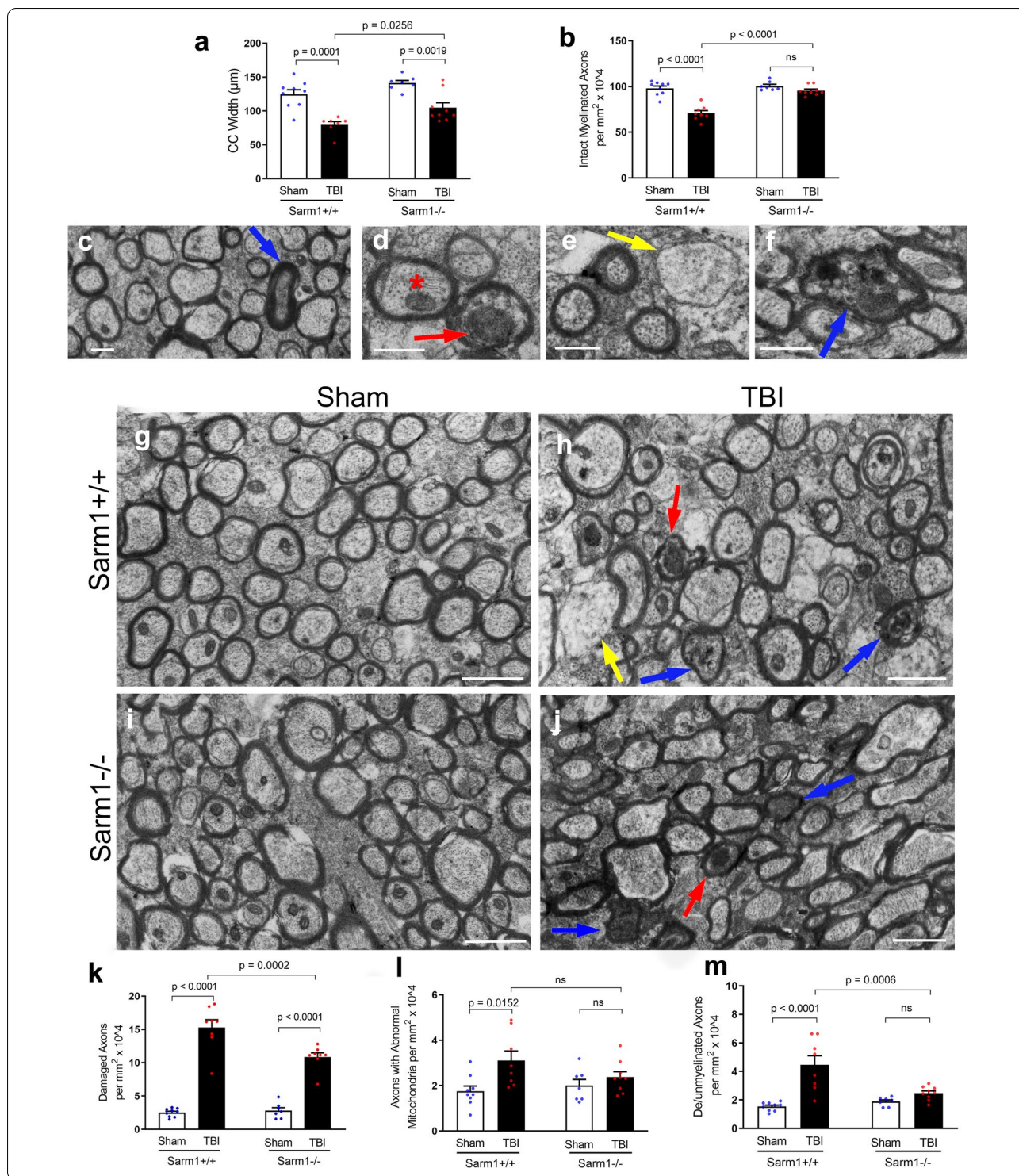
Sarm1 knockout protects against CC atrophy and axon-myelin pathology in chronic TBI

The potential for *Sarm1* inactivation to provide long term axon protection and/or to mitigate post-traumatic neurodegeneration was first evaluated using transmission EM (Fig. 1). Before thin sectioning for EM, sagittal brain slices were osmium-stained to label myelin and examined with bright field microscopy to measure the CC width, which is a clinically relevant measure of white matter pathology in TBI and neurological diseases [20]. Both *Sarm1* WT and *Sarm1* KO mice developed significant CC atrophy by 10 weeks after TBI, yet the extent of atrophy was significantly less in the *Sarm1* KO mice (Fig. 1a). For in-depth analysis of the underlying pathology associated with changes in CC size, the tissue slices were then thin sectioned and imaged by transmission EM at subcellular resolution to examine individual myelinated axons within the same region of the CC. This quantification revealed a significant reduction of intact axons due to TBI in the *Sarm1* WT mice that was rescued in *Sarm1* KO mice (Fig. 1b).

Myelinated axons exhibit subcellular features that can distinguish intact axons from indicators of axon damage including swollen mitochondria, compacted cytoskeletal structure, accumulation of vesicles or debris, or loss of ensheathing myelin (Fig. 1c–f). After the sham procedure, *Sarm1* WT mice illustrate the healthy adult high density of myelinated axons in this anterior region of the CC (Fig. 1g). As previously characterized in this concussive TBI model [52, 61], TBI results in damaged axons that are dispersed among adjacent intact axons and may also exhibit demyelination in *Sarm1* WT mice (Fig. 1h). *Sarm1* KO mice exhibit normal appearing myelinated axons after the sham procedure and dispersed damaged axons after TBI (Fig. 1i, j). Importantly, while both *Sarm1* WT and *Sarm1* KO mice exhibited axon damage

(See figure on next page.)

Fig. 1 *Sarm1* knockout reduces corpus callosum atrophy and axon pathology at 10 weeks post-TBI. **a** *Sarm1* knockout attenuates CC atrophy that develops after TBI. **b** *Sarm1* knockout preserves intact, myelinated axons after TBI. **c–f** Representative images of pathological features from high resolution electron microscopy in CC sagittal sections. **c** Example from a *Sarm1* WT sham mouse to show the cytoskeleton, mitochondria and surrounding myelin sheath of intact axons in contrast with a rare damaged axon with a densely compacted cytoskeleton (blue arrow). **d** *Sarm1* WT TBI mouse example of an axon with an abnormally large mitochondrion (red arrow) and an axon with a typical mitochondrion (red asterisk). Mitochondria were considered abnormal when swollen to > 50% of the axon area. **e** Demyelinated axon (yellow arrow) lacking ensheathing myelin but with otherwise intact cytoskeleton in a *Sarm1* WT TBI mouse. **f** Damaged axon (blue arrow) with vesicle accumulation and cytoskeletal breakdown in a *Sarm1* KO TBI mouse. **g–j** Representative electron microscopy images from CC sagittal sections for *Sarm1* WT sham (**g**) and TBI (**h**) mice in comparison with *Sarm1* KO sham (**i**) and TBI (**j**) mice. Arrows identify examples of damaged axons with accumulated vesicles and/or compacted cytoskeleton (blue), abnormal mitochondria (red), or demyelination (yellow). **k–m** Quantification of axon and myelin pathology at 10 weeks after TBI or sham procedure. *Sarm1* knockout reduces chronic stage axon damage (**k**), normalizes mitochondria morphology (**l**), and eliminates TBI-induced demyelinated component of de/unmyelinated axons (M). *Sarm1* WT: n = 9 sham, n = 8 TBI. *Sarm1* KO: n = 7 sham, n = 9 TBI. ns = not significant. Further statistical details are provided in Additional File 1: Table S1. **c–f** scale bars = 0.5 μ m. **g–j**, scale bars = 1 μ m



after TBI, *Sarm1* inactivation significantly reduced the frequency of damaged myelinated axons (Fig. 1k). Axons with abnormal mitochondria were increased after TBI only in *Sarm1* WT mice yet the *Sarm1* KO reduction of mitochondrial pathology relative to *Sarm1* WT did

not reach significance (Fig. 1l). Finally, *Sarm1* inactivation significantly reduced the frequency of TBI-induced demyelination relative to *Sarm1* WT mice and normalized the frequency to sham levels in *Sarm1* KO mice (Fig. 1m).

Longitudinal in vivo MRI detects CC atrophy after TBI and attenuation by *Sarm1* knockout

Longitudinal MRI studies were conducted to advance the translational impact while further evaluating the effects of *Sarm1* inactivation on white matter integrity and CC atrophy. Each mouse was scanned prior to injury (i.e., baseline), and with follow up scans at acute and chronic stages after TBI. While DTI measures of white matter integrity have long been effectively used for analysis of adult mouse CC [79, 82], volume measurements have only recently been validated for quantification of atrophy and hypertrophy of the relatively small structures of adult mouse brains [3, 9]; Therefore, an initial cross-sectional in vivo study was conducted in C57BL/6 mice to optimize the MRI outcome measures. DTI analysis at 10 weeks after sham or TBI demonstrated significant changes after TBI in CC integrity while high resolution PD-w volumetrics detected significant CC atrophy that was validated by post-imaging neuropathology (Additional File 1: Figure S2).

Longitudinal MRI studies were then conducted to compare *Sarm1* WT and *Sarm1* KO mice. Volumetric analysis showed significant atrophy of the CC between baseline and 10 weeks in *Sarm1* WT mice (Fig. 2a–c) that was attenuated in *Sarm1* KO (Fig. 2d–f), in agreement with the histological results (Fig. 1A). Conversely, MRI shows no significant change in CC volume from baseline to 3 days post-injury (*Sarm1* WT $p=0.6773$; *Sarm1* KO $p=0.1570$), when prior histology has shown no significant CC atrophy [52]. DTI detected reduced white matter integrity across time points after TBI based on reduced fractional anisotropy (FA) in both *Sarm1* WT mice (Fig. 2g, i) and *Sarm1* KO mice (Fig. 2h, i). Progressive decrease in FA was driven by decreased axial diffusivity (AD) at 3 days post-TBI (Fig. 2j) and subsequent elevation of radial diffusivity (RD) at 10 weeks post-TBI (Fig. 2k). *Sarm1* genotype resulted in a significant effect of higher AD values in *Sarm1* KO mice (Fig. 2j).

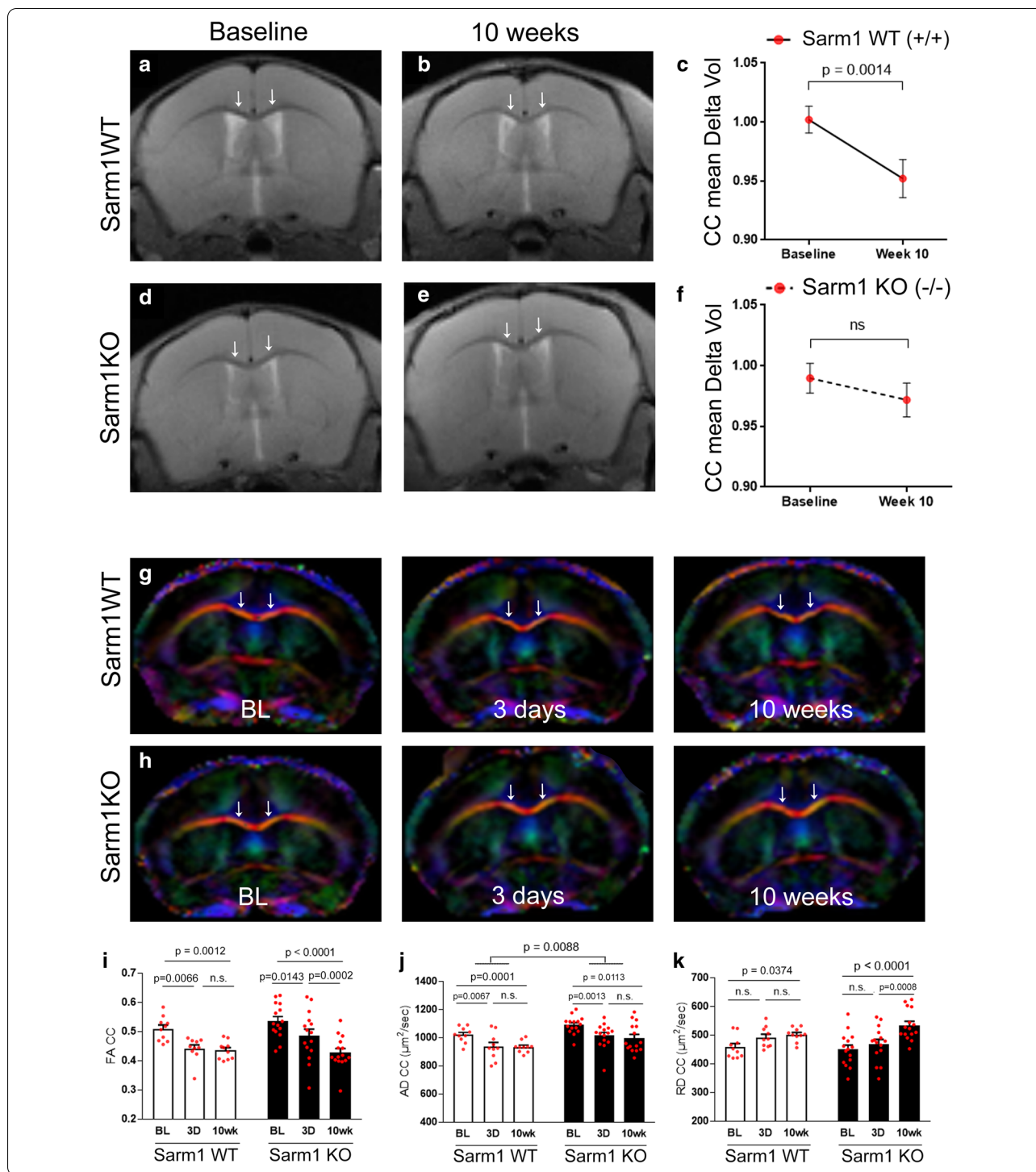
Immunohistochemistry shows reduced neuroinflammation in addition to reduced CC atrophy, axon damage and myelin loss after TBI in *Sarm1* knockout mice

Microglia and astrocyte responses have been linked to chronic white matter damage and atrophy [41, 45, 46, 50, 61, 83]. Therefore, immunohistochemistry was used to evaluate CC atrophy and for analysis of a larger areas for myelination effects in regions with persistent axon damage (Fig. 3a–d) to then examine CC neuroinflammation in adjacent sections (Fig. 4). CC width was measured in coronal sections with myelin immunolabeled for MOG and cytoarchitecture was evaluated using DAPI to stain nuclei (Fig. 3e; Additional File 1: Figure S2). CC width was reduced at 10 weeks after TBI in comparison with sham mice (Fig. 3e). Quantification of the pixel area of MOG immunoreactivity within the CC showed TBI-induced loss of myelin (Fig. 3f). Axon damage was detected as axonal swellings immunolabeled for β -APP (Fig. 3b, d insets). *Sarm1* KO mice had significantly less CC atrophy and less myelin loss and axon damage after TBI as compared to *Sarm1* WT mice (Fig. 3e–g). These findings are in agreement with the EM results for TBI-induced myelinated axon loss and demyelination of intact axons, which both contribute to MOG immunolabeling and are attenuated by *Sarm1* knockout (Fig. 1b, k, m).

Neuroinflammation was estimated by immunolabeling for reactive astrocytes and microglia using GFAP and IBA1, respectively (Fig. 4). TBI resulted in more intense immunoreactivity of individual cells and an increase of overall immunolabeling for both GFAP and IBA1 (Fig. 4a–g). Immunolabeling within the CC after TBI was reduced in *Sarm1* KO mice for GFAP (Fig. 4h) but not for IBA1 (Fig. 4i). Further analysis to count the IBA1 immunolabeled cells within the CC revealed that *Sarm1* inactivation reduced microglia with either a resting state morphology (Fig. 4j) or an activated morphology (Fig. 4k) after TBI. Taken together, these results show that the reduction in CC atrophy and myelin loss seen in *Sarm1* KO mice after TBI was accompanied by a reduced neuroinflammatory response.

(See figure on next page.)

Fig. 2 Progression of corpus callosum atrophy after TBI is sufficient for MRI detection in live mice and is attenuated by *Sarm1* knockout. **a–c** TBI induces significant CC atrophy in *Sarm1* WT mice. High resolution PD-weighted images showing the coronal view at the level of the impact site at baseline (**a**, before surgery) and at 10 weeks (**b**) post-TBI/sham procedures. Quantification of volume change in CC regions under the impact site (**c**). **d–f** In *Sarm1* KO mice, CC atrophy is not detected in representative high resolution PD-weighted images (**d**, **e**) or based on changes in CC volume (**f**). **g–h** Direction encoded color images of diffusion tensor imaging (DTI) from a longitudinal MRI series at baseline (BL) and again at 3 days and 10 weeks post-TBI or sham procedures. Colors represent fiber directions as red (medial–lateral), blue (anterior–posterior), and green (superior–inferior). **i–k** Quantification of DTI measures reveals a chronic progression of CC pathology following TBI. Fractional anisotropy (FA) significantly decreases over time following TBI (**i**). The acute change is driven by a decrease in axial diffusivity (AD) between baseline and 3 days (**j**). *Sarm1* KO mice have significantly higher AD values than *Sarm1* WT mice (**j**). The FA at 10 weeks corresponds with a delayed increase in radial diffusivity (RD) in *Sarm1* KO mice (**k**). Arrows indicate medial CC regions. *Sarm1* WT: $n = 10$ TBI; *Sarm1* KO: $n = 15$ TBI. ns = not significant. Further statistical details are provided in Additional File 1: Table S2



Sarm1 knockout improves functional outcome measures in chronic stage TBI

Behavioral assessments targeting CC axons were selected to test whether the beneficial effects of *Sarm1* inactivation on TBI pathology translated to improved

functional outcome measures. This TBI model did not cause overt symptoms at any time out through 10 weeks post-TBI. Therefore, an initial set of experiments in C57BL/6 mice evaluated two assays associated with CC axon-myelin pathology to determine whether

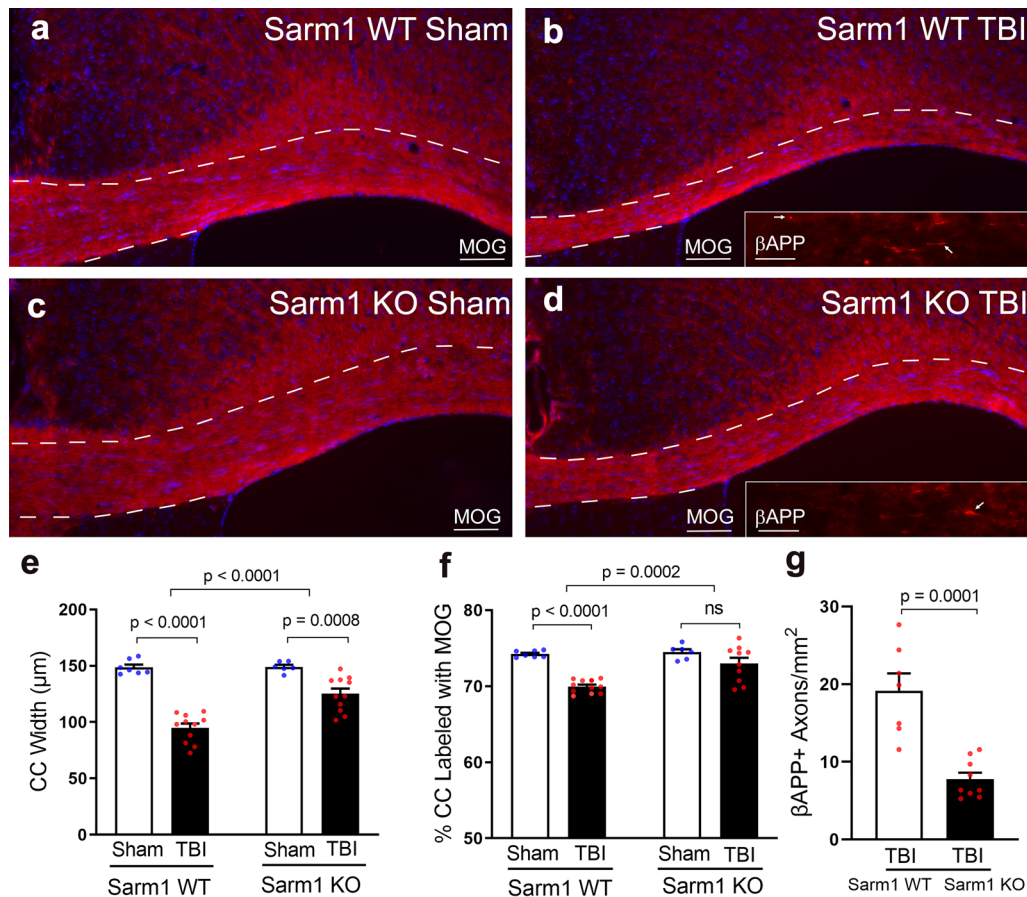


Fig. 3 *Sarm1* knockout reduces corpus callosum atrophy, myelin loss, and axon damage at 10 weeks post-TBI. **a–d** Representative images from CC coronal sections of *Sarm1* WT and *Sarm1* KO mice after sham or TBI procedures. Myelin is detected with immunolabeling for MOG (red). DAPI nuclear stain is shown in blue. Insets show axonal swellings with β -APP immunoreactivity (examples indicated by arrows). CC borders are indicated by dashed lines. **e** *Sarm1* knockout attenuates CC atrophy, which is quantified based on the CC width. **f** TBI results in significant myelin loss as detected by reduced MOG immunoreactivity. Myelin loss after TBI is significantly reduced in *Sarm1* KO mice compared to *Sarm1* WT mice. **g** Axon damage in TBI mice was significantly reduced in *Sarm1* KO mice compared to *Sarm1* WT mice. MOG quantification included *Sarm1* WT: $n = 7$ sham, $n = 11$ TBI; *Sarm1* KO: $n = 6$ sham, $n = 11$ TBI. β -APP quantification included *Sarm1* WT: $n = 6$ TBI; *Sarm1* KO: $n = 9$ TBI. ns = not significant. Further statistical details are provided in Additional File 1: Table S3. Scale bars **a–d** = 100 μ m, insets **b, d** = 25 μ m

either assay revealed deficits during this late phase of TBI. Miss-step wheel running is a motor skill task that engages CC axons and is sensitive to myelination status [36, 60, 82]. C57BL/6 mice showed a deficit in learning to run rapidly on the Miss-step wheels after TBI as compared to sham mice (Additional File 1: Figure S3). C57BL/6 mice with CC pathology from experimental demyelination or repetitive mild TBI exhibit social interaction deficits [62, 95]. However, with the current single impact concussive model of TBI, C57BL/6 mice did not show social interaction deficits (Additional File 1: Figure S4). Based on the results of these assays, the Miss-step wheel task was selected for functional

assessment of TBI deficits in *Sarm1* WT versus *Sarm1* KO mice.

Motor learning and performance on the Miss-step wheels was assessed in *Sarm1* WT and *Sarm1* KO mice from 8 to 10 weeks post-TBI. *Sarm1* KO mice ran at a faster average velocity compared to *Sarm1* WT mice during the learning phase of the assay although this improvement did not reach statistical significance ($p = 0.0821$) (Fig. 5a). Further analysis of running parameters showed that *Sarm1* KO mice ran on the wheels more times during the learning phase compared to *Sarm1* WT mice (Fig. 5b). Additionally, the cumulative distance traveled by *Sarm1* KO mice during the

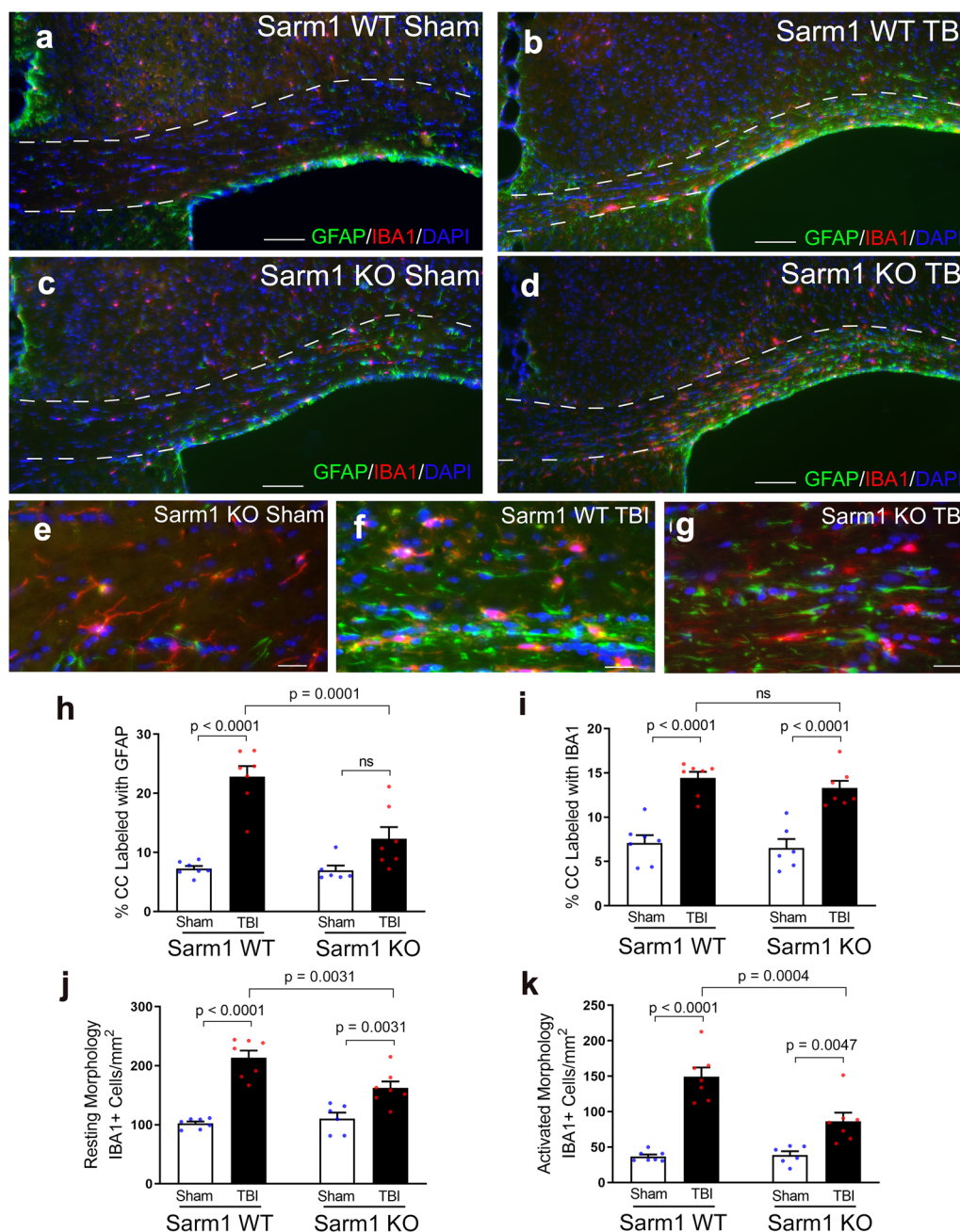


Fig. 4 *Sarm1* knockout reduces neuroinflammation at 10 weeks post-TBI. **a–d** Representative images from CC coronal sections of *Sarm1* WT (**a, b**) and *Sarm1* KO (**c, d**) mice after sham (**a, c**) or TBI (**b, d**) procedures. Neuroinflammation is detected with markers of astrocytes (GFAP, green) and microglia (IBA1, red). DAPI nuclear stain shown in blue. The CC borders are indicated by dashed lines. **e–g** Higher magnification examples of astrocyte (GFAP) and microglia (IBA1) morphology. In sham mice (**e**), astrocytes and microglia exhibit homeostatic morphology with thin processes. Following TBI (**f, g**), reactive astrocytes and microglia have intensely immunolabeled cell bodies and shorter, thicker, processes. **h** *Sarm1* knockout significantly reduced astrogliosis after TBI, based on GFAP immunolabeling within the CC area. **i** The microglial response also indicated CC neuroinflammation after TBI, based on IBA1 immunolabeling, but did not detect differences due to *Sarm1* inactivation. **j–k** More detailed counting of IBA1 immunolabeled (+) cells revealed that *Sarm1* loss significantly reduced the frequency of both resting (**j**) and activated (**k**) microglia after TBI. *Sarm1* WT: n = 7 sham, n = 7 TBI. *Sarm1* KO: n = 6 sham, n = 7 TBI. ns = not significant. Further statistical details are provided in Additional File 1: Table S3. **a–d**, scale bars = 100 μ m. **e–g**, scale bars = 25 μ m

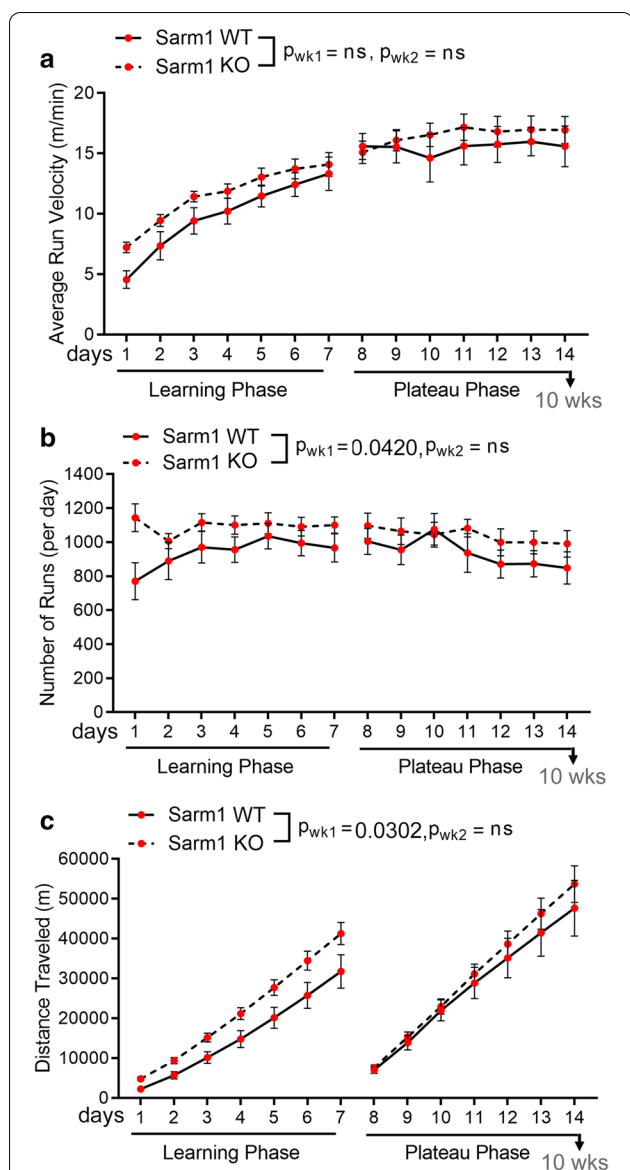


Fig. 5 *Sarm1* knockout improves motor learning in chronic stage TBI. Miss-step wheels have irregularly spaced rungs to assess motor skill learning (week 1) followed by a plateau phase (week 2) that tests bilateral sensorimotor function. **a** *Sarm1* KO mice more quickly learn to run at a faster average velocity compared to *Sarm1* WT mice, but this improvement does not reach statistical significance ($p = 0.0821$). **b** *Sarm1* KO mice run on the wheels more frequently than *Sarm1* WT during the learning phase. **c** Running behavior accumulates to increased total distance traveled during the learning phase in *Sarm1* KO mice compared to *Sarm1* WT mice. There were no statistically significant differences between genotypes in the three measures during the plateau phase (**a–c**). *Sarm1* WT: $n = 9$ TBI. *Sarm1* KO: $n = 15$ TBI. ns = not significant. Further statistical details are provided in Additional File 1: Table S4

learning phase is further for *Sarm1* KO mice than for *Sarm1* WT mice (Fig. 5c).

Sleep behavior was selected in place of social interaction as a highly translational assessment for post-traumatic neurodegeneration (Fig. 6). Sleep disorders are common in patients with chronic TBI and sleep patterns may contribute to neurodegeneration, particularly white matter degeneration [2, 66, 75]. Sleep data was analyzed for *Sarm1* WT and *Sarm1* KO mice during two light/dark cycles. In *Sarm1* WT mice, TBI causes an overall difference from shams in the percent of time spent sleeping (Fig. 6a). This difference was not found in *Sarm1* KO mice (Fig. 6b). More specifically, *Sarm1* WT mice slept less during the lighted period that is the sleep phase for nocturnal mice (Fig. 6c) without a change during the awake phase (Fig. 6d). *Sarm1* KO mice did not exhibit a sleep deficit after TBI, as compared to shams (Fig. 6c, d).

Discussion

The combined results from this study support a direct role of axonal injury in post-traumatic neurodegeneration and provide key pre-clinical evidence for TBI as a clinical indication for treatments to inhibit SARM1. Genetic inactivation of the gene for SARM1, which drives a conserved axon degeneration pathway, had a beneficial effect on chronic white matter injury after TBI. Analysis of CC atrophy with MRI, which is used clinically as a measure of post-traumatic neurodegeneration, was an effective outcome measure in mice. Complementary neuropathological techniques validated CC atrophy and demonstrated that inactivation of the *Sarm1* gene had beneficial effects on chronic stage axon damage, demyelination, and neuroinflammation. Importantly, *Sarm1* knockout preserved healthy axons and prevented the progression of CC atrophy after TBI. *Sarm1* knockout also improved motor learning and normalized time spent sleeping which, together with the pathological and radiological benefits, indicate improved outcome trajectory after TBI.

The current study is the first to use MRI as a translational measure of CC atrophy and to show beneficial effects of *Sarm1* inactivation at a chronic TBI stage. Based on histological measures of CC width, our prior studies in this TBI model did not detect significant CC atrophy at 3 days or at 1, 2, 4 or 6 weeks post-injury [52, 61]. In contrast, significant CC atrophy was evident by histological measures at the longer time point of 8 weeks post-TBI [52, 53]. CC atrophy is an important clinical indicator of post-traumatic neurodegeneration that is associated with chronic stage TBI [30]. We now show significant CC atrophy in live mice using quantitative MRI at 10 weeks post-injury that is validated by neuropathology in C57BL/6 mice (Additional File 1:

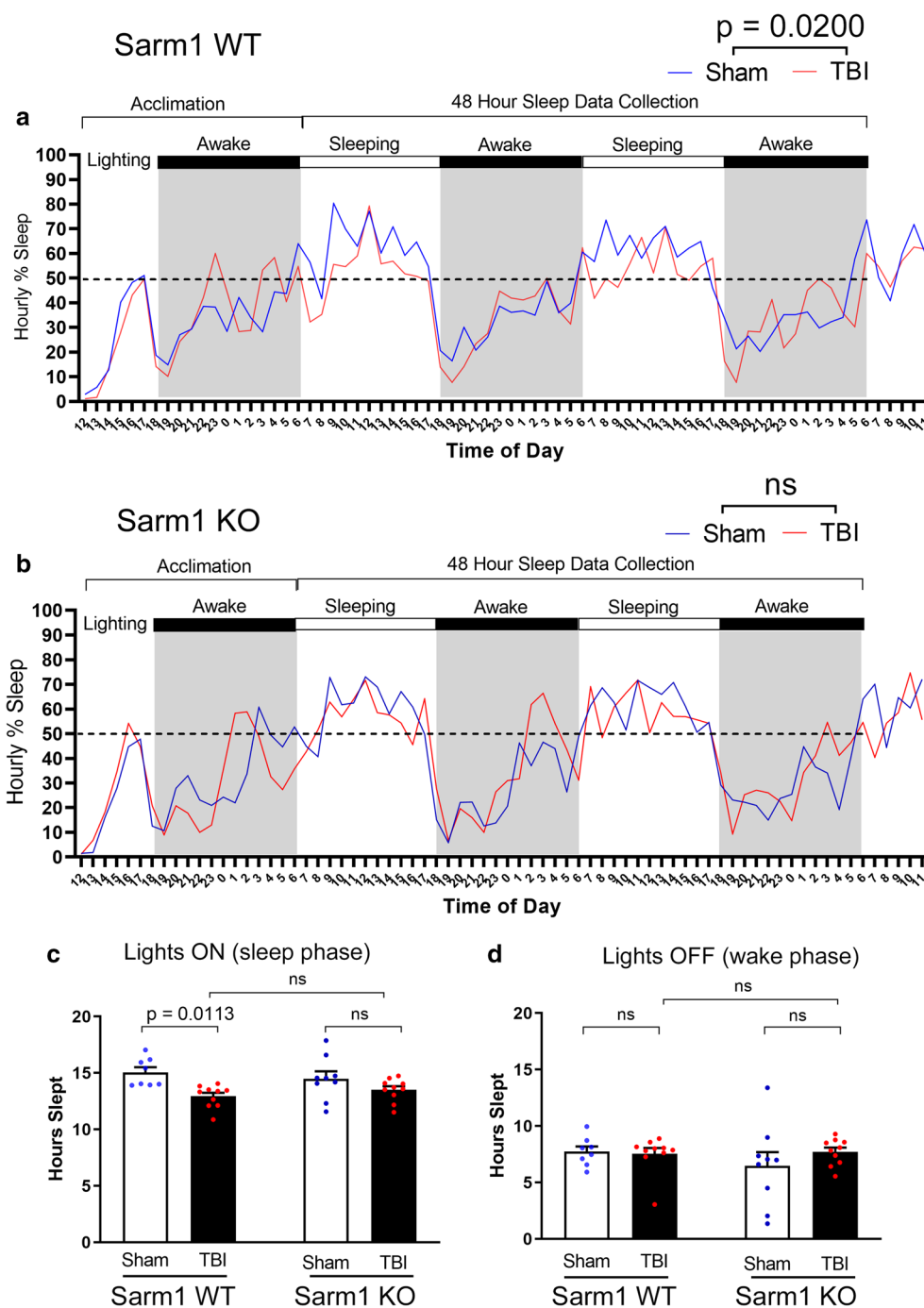


Fig. 6 *Sarm1* knockout normalizes time spent sleeping in the chronic stage of TBI: mice were single housed in cages equipped with a PiezoSleep mouse behavioral tracking system for 72 h during the eighth week after TBI. **a–b** Mice were acclimated for 18 h. Statistical analysis focused on data collected during 48 h across two complete cycles of lights on (white bars) and lights off (dark bars and gray background). Recordings continued for a subsequent 6 h to show the final wake/sleep transition. In *Sarm1* WT mice (**a**), the time spent sleeping per hour is significantly different between sham and TBI, with the injured mice appearing to sleep less during the normal sleeping period when lights are on. In *Sarm1* KO mice (**b**) the sleep pattern was not different between sham and TBI conditions during the 48 h data collection period. **c** TBI significantly reduced the time spent sleeping for *Sarm1* WT mice during the normal sleeping period when lights are on. *Sarm1* KO mice did not exhibit sleep loss after TBI. **d** During the dark period, sleep time was not different based on injury or genotype. *Sarm1* WT: n = 8 sham, n = 10 TBI. *Sarm1* KO: n = 9 sham, n = 10 TBI. ns = not significant. Further statistical details are provided in Additional File 1: Table S5

Figure S2) and in *Sarm1* WT mice (Figs. 1a, 2c, 3e). Significantly, at this 10 week time point, the MRI and neuropathology measures of CC atrophy are attenuated in *Sarm1* KO mice (Figs. 1a, 2f, 3e).

Longitudinal MRI studies of the CC in *Sarm1* WT and KO mice included analysis for DTI FA as a measure of white matter microstructural integrity [91, 94]. Reduced FA values indicated an injury effect at 3 days and at 10 weeks after TBI, as compared to baseline (Fig. 2i–k; Additional File 1: Figure S2). A main effect of *Sarm1* genotype was only observed for the AD parameter (Fig. 2j) that is most often associated with axonal anisotropy within white matter voxels. Interpreting reduced AD as an indicator of axon pathology and increased RD as an indicator of myelin pathology can be useful when each pathology predominates [79, 93]. The presence of simultaneous pathology of axon damage and demyelination is more difficult to detect and interpret using DTI, and is further complicated in the presence of significant edema or neuroinflammation [91, 93]. Histological measures confirm the presence of simultaneous axon damage, demyelination, and neuroinflammation at 10 weeks after TBI along with significant reduction of each pathology in *Sarm1* KO mice (Figs. 1, 3, 4), which is not fully appreciated using the DTI parameters (Fig. 2i–k). Improved detection of axon damage may be possible in future studies based on recent advances in multidimensional MRI to detect diffuse axonal injury lesions in postmortem human TBI [10].

Prior studies have shown significant axon protection in *Sarm1* KO mice in the acute (2 h–3 days) or chronic (2–6 months) phase after closed head TBI based on β -amyloid precursor protein (β -APP) or neurofilament immunohistochemistry [35, 52, 58], or using Thy1-YFP fluorescence to visualize axonal varicosities [52, 96]. Our prior studies at 8 weeks post-injury using immunohistochemistry for MOG in Thy1-YFP-16 mice crossed to the *Sarm1* line also showed CC atrophy and myelin loss in *Sarm1* WT mice that was not present in *Sarm1* KO mice, but without a significant difference based on genotype [52]. Similar analysis of MOG immunohistochemistry in the current experiments showed that CC atrophy and myelin loss were more evident by 10 weeks in *Sarm1* WT mice with a significant genotype effect of reduction in both pathological features and in axon damage in *Sarm1* KO mice (Fig. 3).

Our EM analysis of axon protection is extremely powerful in providing highly sensitive and specific analysis of axon and myelin pathology at the level of individual axons. Our MRI time points for scans in live mice (Fig. 2) are matched with EM data of axon and myelin pathology at 3 days [52] and 10 weeks (Fig. 1) post-TBI in *Sarm1*

WT and *Sarm1* KO littermates. The current 10 week EM data in *Sarm1* WT and *Sarm1* KO mice (Fig. 1) characterizes the critical chronic TBI stage to demonstrate long term benefit of *Sarm1* knockout for axon and myelin pathology.

The progression of axon and myelin pathology identified by EM in *Sarm1* WT and *Sarm1* KO mice indicates an intriguing interaction across acute (3 days), late (6 weeks), and chronic (10 weeks) stages post-injury. In *Sarm1* WT mice, TBI significantly reduced the intact myelinated axons to 56.6% of sham levels at 3 days [52] and to 72.3% of sham levels at 10 weeks (Fig. 1b). Yet, at the intervening 6 week time point, TBI only reduced the intact myelinated axons to 84.7% of shams, which was not a significant reduction [52]. In addition, corresponding axon damage in *Sarm1* WT mice post-TBI was less frequent at 6 weeks and equated to only 60.4% and 56.9% of the respective 3 day [52] and 10 week levels (Fig. 1k). A possible explanation for this pattern of attenuated pathology at 6 weeks in TBI versus sham *Sarm1* WT mice is that early axon damage may undergo a degree of recovery or stabilization of vulnerable axons between 3 days and 6 weeks post-TBI but subsequently axon damage progresses and leads to significant CC atrophy by 10 weeks post-TBI. Changes in mitochondrial pathology, an early feature of axonal injury [68, 92], also appear in agreement with this possibility. In *Sarm1* WT mice, axons with abnormal mitochondria are significantly increased at 3 days [52] and 10 weeks (Fig. 1l) after TBI but not at 6 weeks post-injury [52]. Importantly, significant benefit from *Sarm1* knockout was observed during the acute (3 day) [52] and chronic (10 week; Fig. 1) stages of more marked axon damage and mitochondrial pathology in *Sarm1* WT mice.

EM quantification of abnormal swollen mitochondria as an early feature of axonal injury linked to Wallerian degeneration [90, 92] has important implications for the SARM1 pathway [37, 48]. Mitochondrial dysfunction challenges axon energy metabolism and creates a vulnerable axon state [37, 68]. Mitochondrial stress, trauma or other insults lead to loss of nicotinamide mononucleotide adenylyl-transferase 2 (NMNAT2), an NAD-synthesizing enzyme, in axons that depletes NAD⁺ and raises the level of its precursor nicotinamide mononucleotide (NMN) [21, 48]. Low NAD⁺ and high NMN levels regulate release of auto-inhibition of SARM1 NADase activity, which further depletes NAD⁺ and axon energy stores [12, 22, 39, 76, 80]. Axons with swollen mitochondria were significantly increased at 3 days after TBI in *Sarm1* WT and *Sarm1* KO mice [52]. Compared to this acute 3 day data, axons with swollen mitochondria were less frequent at 10 weeks but still significantly increased after TBI in *Sarm1* WT mice (Fig. 1), which indicates the

potential for continued activation of SARM1 in chronic TBI.

EM identifies damaged axons based on breakdown and compaction of the cytoskeleton and/or accumulated vesicles due to impaired axonal transport (Fig. 1). The frequency of damaged axons and the effect of *Sarm1* knockout is very similar at the 10 week time point (Fig. 1) as compared to 3 days post-TBI [52]. The slow clearance of degenerating axons in the CNS may play a part in this result [89]. Alternatively, surviving axons may succumb to insults in a late phase after TBI and *Sarm1* knockout may have an ongoing benefit across acute and chronic time points. For example, axons continue to initiate Wallerian degeneration long after stretch injury that models TBI forces [56]. Clinically, persistent neuroinflammation in white matter is associated with axon damage in the CC in human postmortem cases several years after TBI [40].

Finally, EM is the gold standard to quantify demyelination, i.e. loss of the myelin sheath around otherwise healthy axons. TBI-induced demyelination in *Sarm1* WT mice was significantly reduced in *Sarm1* KO mice at 10 weeks so that TBI levels were similar to shams (Fig. 1). *Sarm1* is expressed mainly in neurons but a low level of expression in oligodendrocyte lineage cells could have a role in the lack of TBI-induced demyelination in *Sarm1* KO mice [44]. However, the effect of *Sarm1* inactivation may not be an autonomous effect in myelinating oligodendrocytes as zebrafish studies have shown a glioprotective effect of *Sarm1* deletion is dependent on axon protection [86]. Loss of myelin along otherwise healthy axons can slow information processing speed and desynchronize neural circuits; myelin also protects from insults and provides trophic support to axons [6]. Therefore, demyelination that is resolved by *Sarm1* knockout may have ongoing benefit at 10 weeks post-TBI that can impact axon health and neural circuit function.

Pathological and structural benefits of *Sarm1* knockout were complemented by behavioral studies that show beneficial effects on motor learning and sleep assessments (Figs. 5, 6) [2, 55]. Our results extend beyond previous reports in *Sarm1* KO mice to now examine complex behaviors during the chronic phase post-TBI. Studies in a weight drop model of TBI used the neurological severity score battery of simple tasks from 2 h through 4 weeks post-TBI and found reduced deficits in *Sarm1* KO versus *Sarm1* WT mice only during the first week [35]. Studies of repetitive TBI showed normalization toward sham responses in *Sarm1* KO for motor performance and memory deficits during the first week and context fear discrimination at 4 weeks [58]. With assessments conducted beyond 8 weeks post-TBI, *Sarm1* knockout improved motor learning (Fig. 5) and normalized the time spent sleeping (Fig. 6).

The Miss-step wheel running system (Fig. 5) and the piezoelectric sleep system (Fig. 6) use automated multi-day continuous data collection of spontaneous complex behaviors, which may be advantageous for analysis of subtle deficits after TBI. The piezoelectric sleep system may be particularly beneficial for use in repeated testing for longitudinal studies of sleep to non-invasively screen acute through chronic stages. The Miss-step wheel assessment also is of interest for potential relevance to gait performance deficits, including pace, that have been recently identified in mild TBI patients with persistent symptoms [55].

Limitations of the experimental design should be considered in the interpretation of the results. The *Sarm1* KO mice have been backcrossed to the C57BL/6 strain (see methods) but may harbor genes associated with the embryonic stem cell origin in the 129 background strain [88]. However, the findings regarding axon degeneration in this line of *Sarm1* KO mice have been confirmed in additional *Sarm1* KO mice generated using CRISPR technology [88]. In addition, all experiments in the current study used *Sarm1* WT and *Sarm1* KO littermates to minimize the variability due to genetic background. The assessment of sleep disorders after TBI used a non-invasive screening approach to avoid surgical procedures and electrode placement through skull burr holes that would be required for electrophysiology. The sleep behavior in the *Sarm1* KO mice appears normalized to the sham sleep pattern. Based on these findings, electrophysiological recordings would now be of interest to further validate this sleep assessment method relative to the genetic modification and injury model, and for more in-depth analysis of sleep architecture that could further the translational comparison to sleep disorders in TBI patients. Finally, the neuropathological and radiological analyses focused on white matter, and specifically the CC. Further studies would be of interest to better understand the relationship of axon damage and the progression of white matter pathology relative to broader neural circuits and gray matter pathology, including analysis of synapse loss that is associated with chronic neuroinflammation after TBI [1].

Conclusions

These results demonstrate that genetic inactivation of *Sarm1* improves the outcome trajectory after TBI based on pathological, radiological, and functional measures. These studies advance strategies to develop TBI treatments for axon damage by demonstrating a genetic proof-of-concept of the long-term benefit of *Sarm1* inactivation in mice. The therapeutic potential of SARM1 inhibitors has drawn intense interest and a small

molecule inhibitor of SARM1 has already been developed that recapitulates in vitro aspects of the *Sarm1* KO phenotype [37, 49, 77]. The current studies also highlight CC atrophy as an important outcome measure of white matter degeneration after TBI in mice that may have translational relevance as a biomarker for clinical studies [29]. Our results of *Sarm1* genetic inactivation advance white matter degeneration as a tractable therapeutic target for TBI and chronic traumatic encephalopathy, with potential application to other neurodegenerative diseases including Alzheimer's disease and multiple sclerosis [4, 15, 17, 73].

Supplementary Information

The online version contains supplementary material available at <https://doi.org/10.1186/s40478-021-01193-8>.

Additional file 1.

Acknowledgements

The authors thank Dr. Christina Marion and Dr. Krystal Schaar Valenzuela for technical advice. We appreciate the support of the Center for Neuroscience and Regenerative Medicine Preclinical Models Core, Translational Imaging Core, and Translational Therapeutics Core and the Biomedical Instrumentation Center at the Uniformed Services University.

Author Contributions

D.V.B. and R.C.A. designed studies of chronic TBI in *Sarm1* mice. K.L.R., D.V.B. and R.C.A. designed neuropathological analysis of tissue sections. D.V.B. performed TBI surgical procedures. D.V.B., X.Z. and D.P.M. performed neuropathological procedures. D.V.B. and R.C.A. performed neuropathological analyses. R.C.A., A.K.K. and A.K., B.J.D. and D.V.B. designed longitudinal MRI studies. A.K. and D.V.B. performed MRI studies. A.K.K. performed image processing for MRI studies. D.V.B., A.K.K., A.K. and R.C.A. analyzed MRI data. D.V.B. and G.M.S. performed behavioral studies. D.V.B., R.C.A. and G.M.S. designed and analyzed behavioral studies. R.C.A. secured funding for project. D.V.B. and R.C.A. wrote the manuscript. All authors edited and approved the manuscript.

Funding

These studies were funded by the U.S. Department of Defense and the Uniformed Services University through the UCSF-USUHS Partnership: Brain Injury and Disease Prevention, Treatment, and Research and the Center for Neuroscience and Regenerative Medicine.

Availability of data and material

There are no data files for inclusion in a shared data repository at this time.

Declarations

Competing interests

The authors declare no competing financial interests. Opinions are those of the authors and do not represent the University, the Department of Defense, or the federal government.

Author details

¹Graduate Program in Neuroscience, F. Edward Hebert School of Medicine, Uniformed Services University of the Health Sciences, Bethesda, MD 20814, USA. ²Department of Anatomy, Physiology and Genetics, F. Edward Hebert School of Medicine, Uniformed Services University of the Health Sciences, 4301 Jones Bridge Rd., Bethesda, MD 20814, USA. ³Department of Radiology and Radiological Sciences, F. Edward Hebert School of Medicine, Uniformed Services University of the Health Sciences, Bethesda, MD 20814, USA. ⁴Center for Neuroscience and Regenerative Medicine, F. Edward Hebert School

of Medicine, Uniformed Services University of the Health Sciences, Bethesda, MD 20814, USA. ⁵Biomedical Instrumentation Center, F. Edward Hebert School of Medicine, Uniformed Services University of the Health Sciences, Bethesda, MD 20814, USA. ⁶Present Address: Center for Scientific Review, National Institutes of Health, Bethesda, MD, USA.

Received: 9 March 2021 Accepted: 6 May 2021

Published online: 17 May 2021

References

- Alawiah A, Chalhoub RM, Mallah K, Langley EF, York M, Broome H, Couch C, Adkins D, Tomlinson S (2021) Complement drives synaptic degeneration and progressive cognitive decline in the chronic phase after traumatic brain injury. *J Neurosci* 41:1830–1843. <https://doi.org/10.1523/jneurosci.1734-20.2020>
- Altendahl M, Cotter DL, Staffaroni AM, Wolf A, Mumford P, Cobigo Y, Casaletto K, Elahi F, Ruoff L, Javed S et al (2020) REM sleep is associated with white matter integrity in cognitively healthy, older adults. *PLoS ONE* 15:e0235395. <https://doi.org/10.1371/journal.pone.0235395>
- Anderson RJ, Cook JJ, Delpratt N, Nouis JC, Gu B, McNamara JO, Avants BB, Johnson GA, Badea A (2019) Small animal multivariate brain analysis (SAMBA)—a high throughput pipeline with a validation framework. *Neuroinformatics* 17:451–472. <https://doi.org/10.1007/s12021-018-9410-0>
- Andravizou A, Dardiotis E, Artemiadis A, Sokratous M, Siokas V, Tsouris Z, Aloizou AM, Nikolaidis I, Bakirtzis C, Tsvigoulis G et al (2019) Brain atrophy in multiple sclerosis: mechanisms, clinical relevance and treatment options. *Auto Immun Highlights* 10:7. <https://doi.org/10.1186/s13317-019-0117-5>
- Armstrong RC, Le TQ, Flint NC, Vana AC, Zhou Y-X (2006) Endogenous cell repair of chronic demyelination. *J Neuropathol Exp Neurol* 65:245–256. <https://doi.org/10.1097/01.jnen.0000205142.08716.7e>
- Armstrong RC, Mierzwa AJ, Marion CM, Sullivan GM (2016) White matter involvement after TBI: Clues to axon and myelin repair capacity. *Exp Neurol* 275(Pt 3):328–333. <https://doi.org/10.1016/j.expneurol.2015.02.011>
- Avants BB, Epstein CL, Grossman M, Gee JC (2008) Symmetric diffeomorphic image registration with cross-correlation: evaluating automated labeling of elderly and neurodegenerative brain. *Med Image Anal* 12:26–41. <https://doi.org/10.1016/j.media.2007.06.004>
- Avants BB, Yushkevich P, Pluta J, Minkoff D, Korczykowski M, Detre J, Gee JC (2010) The optimal template effect in hippocampus studies of diseased populations. *Neuroimage* 49:2457–2466. <https://doi.org/10.1016/j.neuroimage.2009.09.062>
- Badea A, Ng KL, Anderson RJ, Zhang J, Miller MI, O'Brien RJ (2019) Magnetic resonance imaging of mouse brain networks plasticity following motor learning. *PLoS ONE* 14:e0216596. <https://doi.org/10.1371/journal.pone.0216596>
- Benjamini D, Iacono D, Komlos ME, Perl DP, Brody DL, Basser PJ (2021) Diffuse axonal injury has a characteristic multidimensional MRI signature in the human brain. *Brain* 144:800–816. <https://doi.org/10.1093/brain/awaa447>
- Blumbers PC, Scott G, Manavis J, Wainwright H, Simpson DA, McLean AJ (1995) Topography of axonal injury as defined by amyloid precursor protein and the sector scoring method in mild and severe closed head injury. *J Neurotrauma* 12:565–572. <https://doi.org/10.1089/neu.1995.12.565>
- Bratkowsky M, Xie T, Thayer DA, Lad S, Mathur P, Yang YS, Danko G, Burdett TC, Danao J, Cantor A et al (2020) Structural and mechanistic regulation of the pro-degenerative NAD hydrolase SARM1. *Cell Rep* 32:107999. <https://doi.org/10.1016/j.celrep.2020.107999>
- Büki A, Povlishock JT (2006) All roads lead to disconnection? Traumatic axonal injury revisited. *Acta Neurochir (Wien)* 148:181–193. <https://doi.org/10.1007/s00701-005-0674-4>
- Chen YH, Sasaki Y, DiAntonio A, Milbrandt J (2021) SARM1 is required in human derived sensory neurons for injury-induced and neurotoxic axon degeneration. *Exp Neurol* 339:113636. <https://doi.org/10.1016/j.expneurol.2021.113636>
- Cole JH, Caan MWA, Underwood J, De Francesco D, van Zoest RA, Wit F, Mutsaerts H, Leech R, Geurtsen GJ, Portegies P et al (2018) No evidence for accelerated aging-related brain pathology in treated

- human immunodeficiency virus: longitudinal neuroimaging results from the comorbidity in relation to AIDS (COBRA) project. *Clin Infect Dis* 66:1899–1909. <https://doi.org/10.1093/cid/cix1124>
16. Cole JH, Leech R, Sharp DJ (2015) Prediction of brain age suggests accelerated atrophy after traumatic brain injury. *Ann Neurol* 77:571–581. <https://doi.org/10.1002/ana.24367>
 17. Daneshvar DH, Goldstein LE, Kiernan PT, Stein TD, McKee AC (2015) Post-traumatic neurodegeneration and chronic traumatic encephalopathy. *Mol Cell Neurosci* 66:81–90. <https://doi.org/10.1016/j.mcn.2015.03.007>
 18. Essuman K, Summers DW, Sasaki Y, Mao X, DiAntonio A, Milbrandt J (2017) The SARM1 toll/interleukin-1 receptor domain possesses intrinsic NAD(+) cleavage activity that promotes pathological axonal degeneration. *Neuron* 93:1334–1343. <https://doi.org/10.1016/j.neuron.2017.02.022>
 19. Fann JR, Ribe AR, Pedersen HS, Fenger-Grøn M, Christensen J, Benros ME, Vestergaard M (2018) Long-term risk of dementia among people with traumatic brain injury in Denmark: a population-based observational cohort study. *Lancet Psychiatry* 5:424–431. [https://doi.org/10.1016/S2215-0366\(18\)30065-8](https://doi.org/10.1016/S2215-0366(18)30065-8)
 20. Ferrazzano P, Yeske B, Mumford J, Kirk G, Bigler EDP, Bowen K, O'Brien N, Rosario B, Beers SR, Rathouz P et al (2021) Brain MRI volumetric measures of functional outcome after severe TBI in Adolescents. *J Neurotrauma*. <https://doi.org/10.1089/neu.2019.6918>
 21. Figley MD, DiAntonio A (2020) The SARM1 axon degeneration pathway: control of the NAD(+) metabolome regulates axon survival in health and disease. *Curr Opin Neurobiol* 63:59–66. <https://doi.org/10.1016/j.conb.2020.02.012>
 22. Figley MD, Gu W, Nanson JD, Shi Y, Sasaki Y, Cunnea K, Malde AK, Jia X, Luo Z, Saikot FK et al (2021) SARM1 is a metabolic sensor activated by an increased NMN/NAD(+) ratio to trigger axon degeneration. *Neuron*. <https://doi.org/10.1016/j.neuron.2021.02.009>
 23. Geisler S, Doan RA, Cheng GC, Cetinkaya-Figgin A, Huang SX, Hoke A, Milbrandt J, DiAntonio A (2019) Vincristine and bortezomib use distinct upstream mechanisms to activate a common SARM1-dependent axon degeneration program. *JCI Insight*. <https://doi.org/10.1172/jci.insight.129920>
 24. Geisler S, Doan RA, Strickland A, Huang X, Milbrandt J, DiAntonio A (2016) Prevention of vincristine-induced peripheral neuropathy by genetic deletion of SARM1 in mice. *Brain* 139:3092–3108. <https://doi.org/10.1093/brain/aww251>
 25. Gerdts J, Brace EJ, Sasaki Y, DiAntonio A, Milbrandt J (2015) SARM1 activation triggers axon degeneration locally via NAD(+) destruction. *Science* 348:453–457. <https://doi.org/10.1126/science.1258366>
 26. Gerdts J, Summers DW, Milbrandt J, DiAntonio A (2016) Axon Self-Destruction: new Links among SARM1, MAPKs, and NAD+ Metabolism. *Neuron* 89:449–460. <https://doi.org/10.1016/j.neuron.2015.12.023>
 27. Gerdts J, Summers DW, Sasaki Y, DiAntonio A, Milbrandt J (2013) Sarm1-mediated axon degeneration requires both SAM and TIR interactions. *J Neurosci* 33:13569–13580. <https://doi.org/10.1523/JNEUROSCI.1197-13.2013>
 28. Gilley J, Orsomando G, Nascimento-Ferreira I, Coleman MP (2015) Absence of SARM1 rescues development and survival of NMNAT2-deficient axons. *Cell Rep* 10:1974–1981. <https://doi.org/10.1016/j.celrep.2015.02.060>
 29. Graham NS, Sharp DJ (2019) Understanding neurodegeneration after traumatic brain injury: from mechanisms to clinical trials in dementia. *J Neurol Neurosurg Psychiatry* 90:1221–1233. <https://doi.org/10.1136/jnnp-2017-317557>
 30. Graham NSN, Jolly A, Zimmerman K, Bourke NJ, Scott G, Cole JH, Schott JM, Sharp DJ (2020) Diffuse axonal injury predicts neurodegeneration after moderate-severe traumatic brain injury. *Brain* 143:3685–3698. <https://doi.org/10.1093/brain/awaa316>
 31. Green RE, Colella B, Maller JJ, Bayley M, Glazer J, Mikulis DJ (2014) Scale and pattern of atrophy in the chronic stages of moderate-severe TBI. *Front Hum Neurosci* 8:67. <https://doi.org/10.3389/fnhum.2014.00067>
 32. Gu Y, Jukkola P, Wang Q, Esparza T, Zhao Y, Brody D, Gu C (2017) Polarity of varicosity initiation in central neuron mechanosensation. *J Cell Biol* 216:2179–2199. <https://doi.org/10.1083/jcb.201606065>
 33. Hayes JP, Bigler ED, Verfaellie M (2016) Traumatic brain injury as a disorder of brain connectivity. *J Int Neuropsychol Soc* 22:120–137. <https://doi.org/10.1017/s1355617715000740>
 34. Hennig J, Nauerth A, Friedburg H (1986) RARE imaging: a fast imaging method for clinical MR. *Magn Reson Med* 3:823–833. <https://doi.org/10.1002/mrm.1910030602>
 35. Henninger N, Bouley J, Sikoglu EM, An J, Moore CM, King JA, Bowser R, Freeman MR, Brown RH Jr (2016) Attenuated traumatic axonal injury and improved functional outcome after traumatic brain injury in mice lacking Sarm1. *Brain* 139:1094–1105. <https://doi.org/10.1093/brain/aww001>
 36. Hibbits N, Pannu R, Wu TJ, Armstrong RC (2009) Cuprizone demyelination of the corpus callosum in mice correlates with altered social interaction and impaired bilateral sensorimotor coordination. *ASN Neuro*. <https://doi.org/10.1042/AN20090032>
 37. Hughes RO, Bosanac T, Mao X, Engber TM, DiAntonio A, Milbrandt J, Devraj R, Krauss R (2021) Small molecule SARM1 inhibitors recapitulate the SARM1(–/–) phenotype and allow recovery of a metastable pool of axons fated to degenerate. *Cell Rep* 34:108588. <https://doi.org/10.1016/j.celrep.2020.108588>
 38. Jang SH, Kim OL, Kim SH, Lee HD (2019) Differences in corpus callosum injury between cerebral concussion and diffuse axonal injury. *Medicine (Baltimore)* 98:e17467. <https://doi.org/10.1097/md.00000000000017467>
 39. Jiang Y, Liu T, Lee CH, Chang Q, Yang J, Zhang Z (2020) The NAD(+) mediated self-inhibition mechanism of pro-neurodegenerative SARM1. *Nature* 588:658–663. <https://doi.org/10.1038/s41586-020-2862-z>
 40. Johnson VE, Stewart JE, Begbie FD, Trojanowski JQ, Smith DH, Stewart W (2013) Inflammation and white matter degeneration persist for years after a single traumatic brain injury. *Brain* 136:28–42. <https://doi.org/10.1093/brain/aww322>
 41. Johnson VE, Stewart W, Smith DH (2013) Axonal pathology in traumatic brain injury. *Exp Neurol* 246:35–43. <https://doi.org/10.1016/j.expneurol.2012.01.013>
 42. Juengst SB, Nabasny A, Terhorst L (2019) Neurobehavioral symptoms in community-dwelling adults with and without chronic traumatic brain injury: differences by age, gender, education, and health condition. *Front Neurol* 10:1210. <https://doi.org/10.3389/fneur.2019.01210>
 43. Kim Y, Zhou P, Qian L, Chuang JZ, Lee J, Li C, Iadecola C, Nathan C, Ding A (2007) MyD88-5 links mitochondria, microtubules, and JNK3 in neurons and regulates neuronal survival. *J Exp Med* 204:2063–2074. <https://doi.org/10.1084/jem.20070868>
 44. Ko KW, Milbrandt J, DiAntonio A (2020) SARM1 acts downstream of neuroinflammatory and necroptotic signaling to induce axon degeneration. *J Cell Biol*. <https://doi.org/10.1083/jcb.201912047>
 45. Kumar A, Loane DJ (2012) Neuroinflammation after traumatic brain injury: opportunities for therapeutic intervention. *Brain Behav Immun* 26:1191–1201. <https://doi.org/10.1016/j.bbi.2012.06.008>
 46. Kwicien JM (2021) The pathogenesis of neurotrauma indicates targets for neuroprotective therapies. *Curr Neuropharmacol*. <https://doi.org/10.2174/1570159x19666210125153308>
 47. Leconte C, Benedetto C, Lentini F, Simon K, Ouazizi C, Taib T, Cho A, Plotkine M, Mongeau R, Marchand-Leroux C et al (2020) Histological and behavioral evaluation after traumatic brain injury in mice: a ten months follow-up study. *J Neurotrauma* 37:1342–1357. <https://doi.org/10.1089/neu.2019.6679>
 48. Loreto A, Hill CS, Hewitt VL, Orsomando G, Angeletti C, Gilley J, Lucci C, Sanchez-Martinez A, Whitworth AJ, Conforti L et al (2019) Mitochondrial impairment activates the Wallerian pathway through depletion of NMNAT2 leading to SARM1-dependent axon degeneration. *Neurobiol Dis*. <https://doi.org/10.1016/j.nbd.2019.104678>
 49. Loring HS, Thompson PR (2019) Emergence of SARM1 as a potential therapeutic target for Wallerian-type diseases. *Cell Chem Biol*. <https://doi.org/10.1016/j.chembiol.2019.11.002>
 50. Lozano D, Gonzales-Portillo GS, Acosta S, de la Pena I, Tajiri N, Kaneko Y, Borlongan CV (2015) Neuroinflammatory responses to traumatic brain injury: etiology, clinical consequences, and therapeutic opportunities. *Neuropsychiatr Dis Treat* 11:97–106. <https://doi.org/10.2147/ndt.S65815>
 51. Mang GM, Nicod J, Emmenegger Y, Donohue KD, O'Hara BF, Franken P (2014) Evaluation of a piezoelectric system as an alternative to electroencephalogram/ electromyogram recordings in mouse sleep studies. *Sleep* 37:1383–1392. <https://doi.org/10.5665/sleep.3936>
 52. Marion CM, McDaniel DP, Armstrong RC (2019) Sarm1 deletion reduces axon damage, demyelination, and white matter atrophy after experimental traumatic brain injury. *Exp Neurol* 321:113040. <https://doi.org/10.1016/j.expneurol.2019.113040>

53. Marion CM, Radomski KL, Cramer NP, Galdzicki Z, Armstrong RC (2018) Experimental traumatic brain injury identifies distinct early and late phase axonal conduction deficits of white matter pathophysiology, and reveals intervening recovery. *J Neurosci* 38:8723–8736. <https://doi.org/10.1523/jneurosci.0819-18.2018>
54. Marmarou CR, Walker SA, Davis CL, Povlishock JT (2005) Quantitative analysis of the relationship between intra-axonal neurofilament compaction and impaired axonal transport following diffuse traumatic brain injury. *J Neurotrauma* 22:1066–1080. <https://doi.org/10.1089/neu.2005.22.1066>
55. Martini DN, Parrington L, Stuart S, Fino PC, King LA (2021) Gait performance in people with symptomatic, chronic mild traumatic brain injury. *J Neurotrauma* 38:218–224. <https://doi.org/10.1089/neu.2020.6986>
56. Maxwell WL, Bartlett E, Morgan H (2015) Wallerian degeneration in the optic nerve stretch-injury model of traumatic brain injury: a stereological analysis. *J Neurotrauma* 32:780–790. <https://doi.org/10.1089/neu.2014.3369>
57. Maxwell WL, Povlishock JT, Graham DL (1997) A mechanistic analysis of nondisruptive axonal injury: a review. *J Neurotrauma* 14:419–440. <https://doi.org/10.1089/neu.1997.14.419>
58. Maynard ME, Redell JB, Zhao J, Hood KN, Vita SM, Kobori N, Dash PK (2020) Sarm1 loss reduces axonal damage and improves cognitive outcome after repetitive mild closed head injury. *Exp Neurol* 327:113207. <https://doi.org/10.1016/j.expneurol.2020.113207>
59. McInnes K, Friesen CL, MacKenzie DE, Westwood DA, Boe SG (2017) Mild Traumatic Brain Injury (mTBI) and chronic cognitive impairment: a scoping review. *PLoS ONE* 12:e0174847. <https://doi.org/10.1371/journal.pone.0174847>
60. McKenzie IA, Ohayon D, Li H, de Faria JP, Emery B, Tohyama K, Richardson WD (2014) Motor skill learning requires active central myelination. *Science* 346:318–322. <https://doi.org/10.1126/science.1254960>
61. Mierzwa AJ, Marion CM, Sullivan GM, McDaniel DP, Armstrong RC (2015) Components of myelin damage and repair in the progression of white matter pathology after mild traumatic brain injury. *J Neuropathol Exp Neurol* 74:218–232. <https://doi.org/10.1097/NEN.000000000000165>
62. Mierzwa AJ, Zhou YX, Hibbits N, Vana AC, Armstrong RC (2013) FGF2 and FGFR1 signaling regulate functional recovery following cuprizone demyelination. *Neurosci Lett* 548:280–285. <https://doi.org/10.1016/j.neulet.2013.05.010>
63. Mountney A, Boutté AM, Cartagena CM, Flerlage WF, Johnson WD, Rho C, Lu XC, Yarnell A, Marciscin S, Sousa J et al (2017) Functional and molecular correlates after single and repeated rat closed-head concussion: indices of vulnerability after brain injury. *J Neurotrauma* 34:2768–2789. <https://doi.org/10.1089/neu.2016.4679>
64. Mouzon B, Bachmeier C, Ojo J, Acker C, Ferguson S, Crynen G, Davies P, Mullan M, Stewart W, Crawford F (2019) Chronic white matter degeneration, but no tau pathology at one-year post-repetitive mild traumatic brain injury in a tau transgenic model. *J Neurotrauma* 36:576–588. <https://doi.org/10.1089/neu.2018.5720>
65. Mustafa Okan Irfanoglu AN, Jeffrey J, Carlo P (2018) TORTOISEv3: Improvements and New Features of the NIH Diffusion MRI Processing Pipeline. ISMRM 25th annual meeting, City
66. Nedergaard M, Goldman SA (2020) Glymphatic failure as a final common pathway to dementia. *Science* 370:50–56. <https://doi.org/10.1126/science.abb8739>
67. Nelson LD, Temkin NR, Dikmen S, Barber J, Giacino JT, Yuh E, Levin HS, McCrea MA, Stein MB, Mukherjee P et al (2019) Recovery after mild traumatic brain injury in patients presenting to us level I trauma centers: a transforming research and clinical knowledge in traumatic brain injury (TRACK-TBI) study. *JAMA Neurol* 76:1049–1059. <https://doi.org/10.1001/jamaneurol.2019.1313>
68. Nikić I, Merkler D, Sorbara C, Brinkoetter M, Kreutzfeldt M, Bareyre FM, Brück W, Bishop D, Misgeld T, Kerschensteiner M (2011) A reversible form of axon damage in experimental autoimmune encephalomyelitis and multiple sclerosis. *Nat Med* 17:495–499. <https://doi.org/10.1038/nm.2324>
69. Nolan AL, Petersen C, Iacono D, Mac Donald CL, Mukherjee P, van der Kouwe A, Jain S, Stevens A, Diamond BR, Wang R et al (2021) Tractography-pathology correlations in traumatic brain injury: a TRACK-TBI study. *J Neurotrauma*. <https://doi.org/10.1089/neu.2020.7373>
70. Osterloh JM, Yang J, Rooney TM, Fox AN, Adalbert R, Powell EH, Sheehan AE, Avery MA, Hackett R, Logan MA et al (2012) dSarm/Sarm1 is required for activation of an injury-induced axon death pathway. *Science* 337:481–484. <https://doi.org/10.1126/science.1223899>
71. Pierpaoli CWL, Irfanoglu MO, Barnett A, Basser P, Chang L-C, Koay C, Pajevic S, Rohde G, Sarlls J, Wu M (2010) TORTOISE: an integrated software package for processing of diffusion MRI data. ISMRM 18th annual meeting, City
72. Rabinowitz AR, Hart T, Whyte J, Kim J (2019) Neuropsychological recovery trajectories in moderate to severe traumatic brain injury: influence of patient characteristics and diffuse axonal injury—erratum. *J Int Neuropsychol Soc* 25:998. <https://doi.org/10.1017/s1355617718000346>
73. Roseborough A, Hachinski V, Whitehead S (2020) White matter degeneration—a treatable target? *JAMA Neurol* 77:793–794. <https://doi.org/10.1001/jamaneurol.2020.0814>
74. Roy S, Butman JA, Pham DL (2017) Robust skull stripping using multiple MR image contrasts insensitive to pathology. *Neuroimage* 146:132–147. <https://doi.org/10.1016/j.neuroimage.2016.11.017>
75. Saksvik SB, Karaliute M, Kallestad H, Follstad T, Asarnow R, Vik A, Håberg AK, Skandsen T, Olsen A (2020) The prevalence and stability of sleep-wake disturbance and fatigue throughout the first year after mild traumatic brain injury. *J Neurotrauma* 37:2528–2541. <https://doi.org/10.1089/neu.2019.6898>
76. Shen C, Vohra M, Zhang P, Mao X, Figley MD, Zhu J, Sasaki Y, Wu H, DiAntonio A, Milbrandt J (2021) Multiple domain interfaces mediate SARM1 autoinhibition. *Proc Natl Acad Sci U S A*. <https://doi.org/10.1073/pnas.2023151118>
77. Simon DJ, Watkins TA (2018) Therapeutic opportunities and pitfalls in the treatment of axon degeneration. *Curr Opin Neurol* 31:693–701. <https://doi.org/10.1097/wco.0000000000000621>
78. Smith DH, Stewart W (2020) “Concussion” is not a true diagnosis. *Nat Rev Neurol* 16:457–458. <https://doi.org/10.1038/s41582-020-0382-y>
79. Song SK, Yoshino J, Le TQ, Lin SJ, Sun SW, Cross AH, Armstrong RC (2005) Demyelination increases radial diffusivity in corpus callosum of mouse brain. *Neuroimage* 26:132–140. <https://doi.org/10.1016/j.neuroimage.2005.01.028>
80. Sporny M, Guez-Haddad J, Khazma T, Yaron A, Dessau M, Shkolnisky Y, Mim C, Isupov MN, Zalk R, Hons M et al (2020) Structural basis for SARM1 inhibition and activation under energetic stress. *Elife*. <https://doi.org/10.7554/eLife.62021>
81. Sturrock RR (1980) Myelination of the mouse corpus callosum. *Neuropathol Appl Neurobiol* 6:415–420. <https://doi.org/10.1111/j.1365-2990.1980.tb00219.x>
82. Sullivan GM, Knutsen AK, Peruzzotti-Jametti L, Korotcov A, Bosomtwi A, Dardzinski BJ, Bernstock JD, Rizzi S, Edenhofer F, Pluchino S et al (2020) Transplantation of induced neural stem cells (iNSCs) into chronically demyelinated corpus callosum ameliorates motor deficits. *Acta Neuropathol Commun* 8:84. <https://doi.org/10.1186/s40478-020-00960-3>
83. Sullivan GM, Mierzwa AJ, Kijpalsalratana N, Tang H, Wang Y, Song SK, Selwyn R, Armstrong RC (2013) Oligodendrocyte lineage and subventricular zone response to traumatic axonal injury in the corpus callosum. *J Neuropathol Exp Neurol* 72:1106–1125. <https://doi.org/10.1097/NEN.000000000000009>
84. Summers DW, DiAntonio A, Milbrandt J (2014) Mitochondrial dysfunction induces Sarm1-dependent cell death in sensory neurons. *J Neurosci* 34:9338–9350. <https://doi.org/10.1523/JNEUROSCI.0877-14.2014>
85. Summers DW, Gibson DA, DiAntonio A, Milbrandt J (2016) SARM1-specific motifs in the TIR domain enable NAD⁺ loss and regulate injury-induced SARM1 activation. *Proc Natl Acad Sci U S A* 113:E6271–E6280. <https://doi.org/10.1073/pnas.1601506113>
86. Tian W, Czopka T, López-Schier H (2020) Systemic loss of Sarm1 protects Schwann cells from chemotoxicity by delaying axon degeneration. *Commun Biol* 3:49. <https://doi.org/10.1038/s42003-020-0776-9>
87. Tobin JE, Xie M, Le TQ, Song SK, Armstrong RC (2011) Reduced axonopathy and enhanced remyelination after chronic demyelination in fibroblast growth factor 2 (Fgf2)-null mice: differential detection with diffusion tensor imaging. *J Neuropathol Exp Neurol* 70:157–165. <https://doi.org/10.1097/NEN.0b013e31820937e4>
88. Uccellini MB, Bardina SV, Sánchez-Aparicio MT, White KM, Hou YJ, Lim JK, García-Sastre A (2020) Passenger mutations confound phenotypes

- of SARM1-deficient mice. *Cell Rep* 31:107498. <https://doi.org/10.1016/j.celrep.2020.03.062>
89. Vargas ME, Barres BA (2007) Why is Wallerian degeneration in the CNS so slow? *Annu Rev Neurosci* 30:153–179. <https://doi.org/10.1146/annurev.neuro.30.051606.094354>
90. Vial JD (1958) The early changes in the axoplasm during wallerian degeneration. *J Biophys Biochem Cytol* 4:551–555. <https://doi.org/10.1083/jcb.4.5.551>
91. Wang X, Cusick MF, Wang Y, Sun P, Libbey JE, Trinkaus K, Fujinami RS, Song SK (2014) Diffusion basis spectrum imaging detects and distinguishes coexisting subclinical inflammation, demyelination and axonal injury in experimental autoimmune encephalomyelitis mice. *NMR Biomed* 27:843–852. <https://doi.org/10.1002/nbm.3129>
92. Williams PR, Marincu B-N, Sorbara CD, Mahler CF, Schumacher A-M, Griesbeck O, Kerschensteiner M, Misgeld T (2014) A recoverable state of axon injury persists for hours after spinal cord contusion in vivo. *Nat Commun* 5:5683. <https://doi.org/10.1038/ncomms6683>
93. Xie M, Tobin JE, Budde MD, Chen CI, Trinkaus K, Cross AH, McDaniel DP, Song SK, Armstrong RC (2010) Rostrocaudal analysis of corpus callosum demyelination and axon damage across disease stages refines diffusion tensor imaging correlations with pathological features. *J Neuropathol Exp Neurol* 69:704–716. <https://doi.org/10.1097/NEN.0b013e3181e3de90>
94. Yaghouby F, Donohue KD, O'Hara BF, Sunderam S (2016) Noninvasive dissection of mouse sleep using a piezoelectric motion sensor. *J Neurosci Methods* 259:90–100. <https://doi.org/10.1016/j.jneumeth.2015.11.004>
95. Yu F, Shukla DK, Armstrong RC, Marion CM, Radomski KL, Selwyn RG, Dardzinski BJ (2017) Repetitive model of mild traumatic brain injury produces cortical abnormalities detectable by magnetic resonance diffusion imaging, histopathology, and behavior. *J Neurotrauma* 34:1364–1381. <https://doi.org/10.1089/neu.2016.4569>
96. Ziogas NK, Koliatsos VE (2018) Primary traumatic axonopathy in mice subjected to impact acceleration: a reappraisal of pathology and mechanisms with high-resolution anatomical methods. *J Neurosci* 38:4031–4047. <https://doi.org/10.1523/JNEUROSCI.2343-17.2018>

Publisher's Note

Springer Nature remains neutral with regard to jurisdictional claims in published maps and institutional affiliations.

Ready to submit your research? Choose BMC and benefit from:

- fast, convenient online submission
- thorough peer review by experienced researchers in your field
- rapid publication on acceptance
- support for research data, including large and complex data types
- gold Open Access which fosters wider collaboration and increased citations
- maximum visibility for your research: over 100M website views per year

At BMC, research is always in progress.

Learn more biomedcentral.com/submissions

